Luminous components

- Active Galactic Nucleus (AGN)
- Stars
- Interstellar Medium (ISM)
- ...

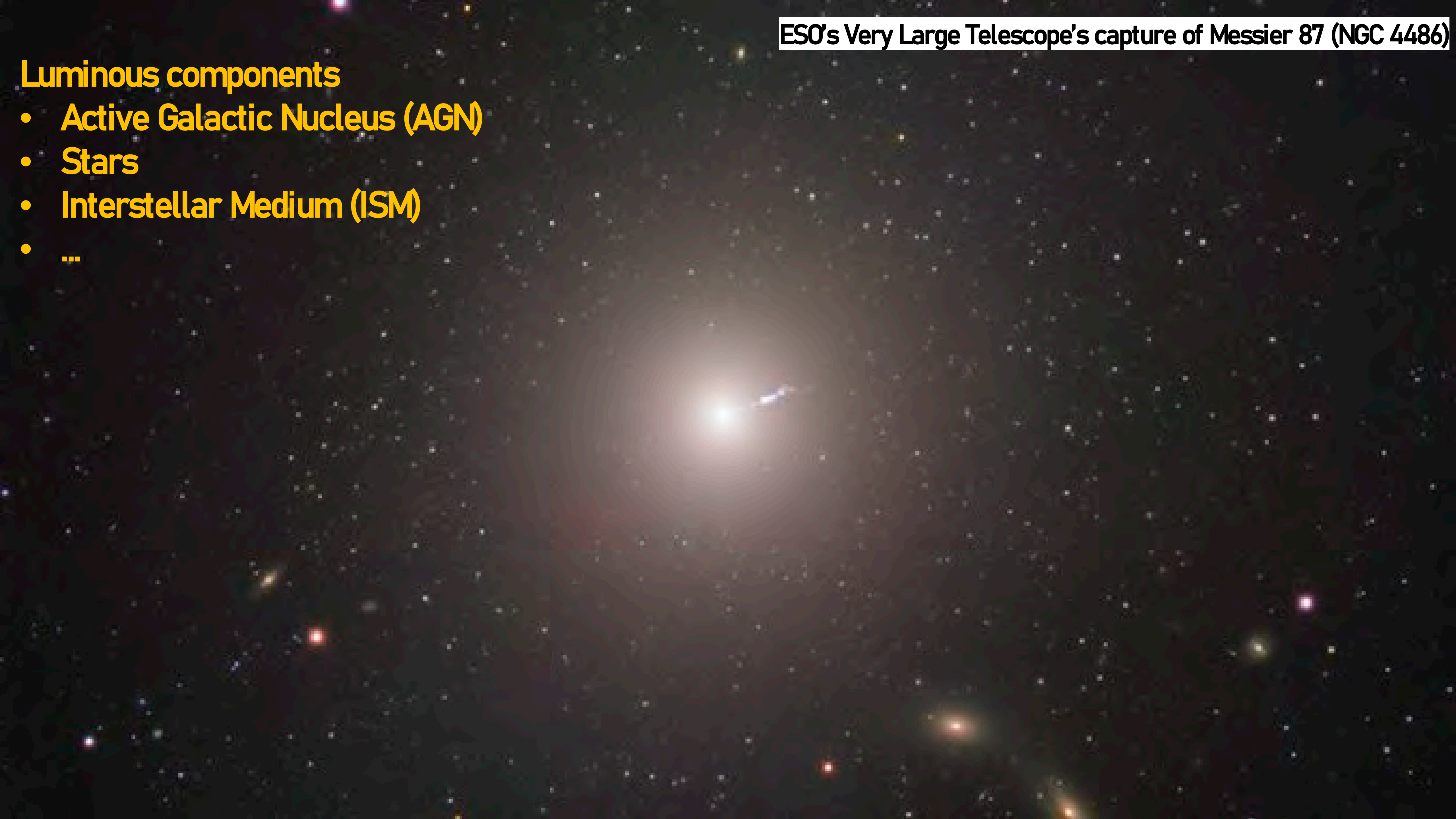

ESO's Very Large Telescope's capture of Messier 87 (NGC 4486)

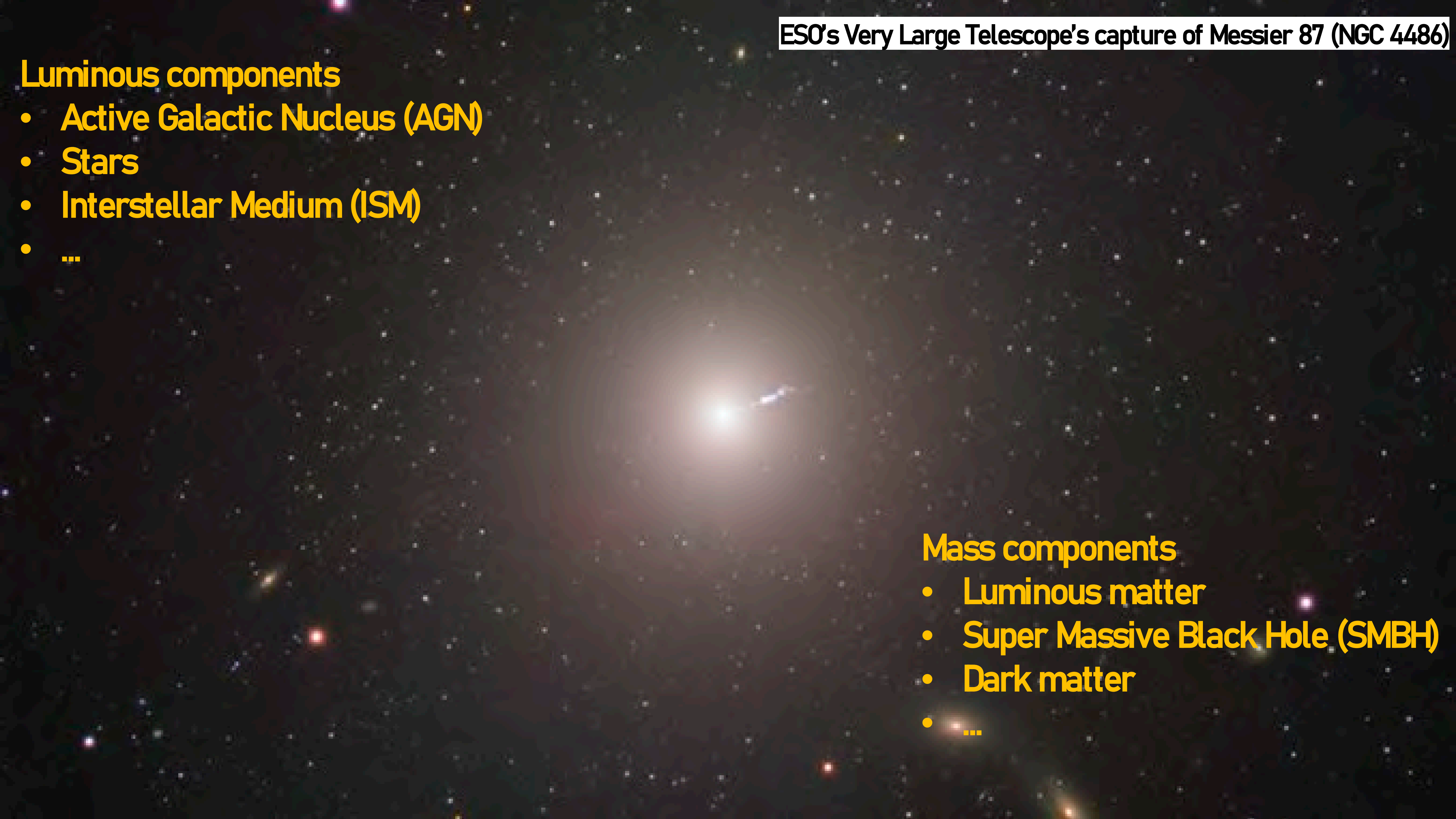
ESO's Very Large Telescope's capture of Messier 87 (NGC 4486)
Luminous components
• Active Galactic Nucleus (AGN)
• Stars
• Interstellar Medium (ISM)
• ...
Mass components
• Luminous matter
• Super Massive Black Hole (SMBH)
• Dark matter
• ...

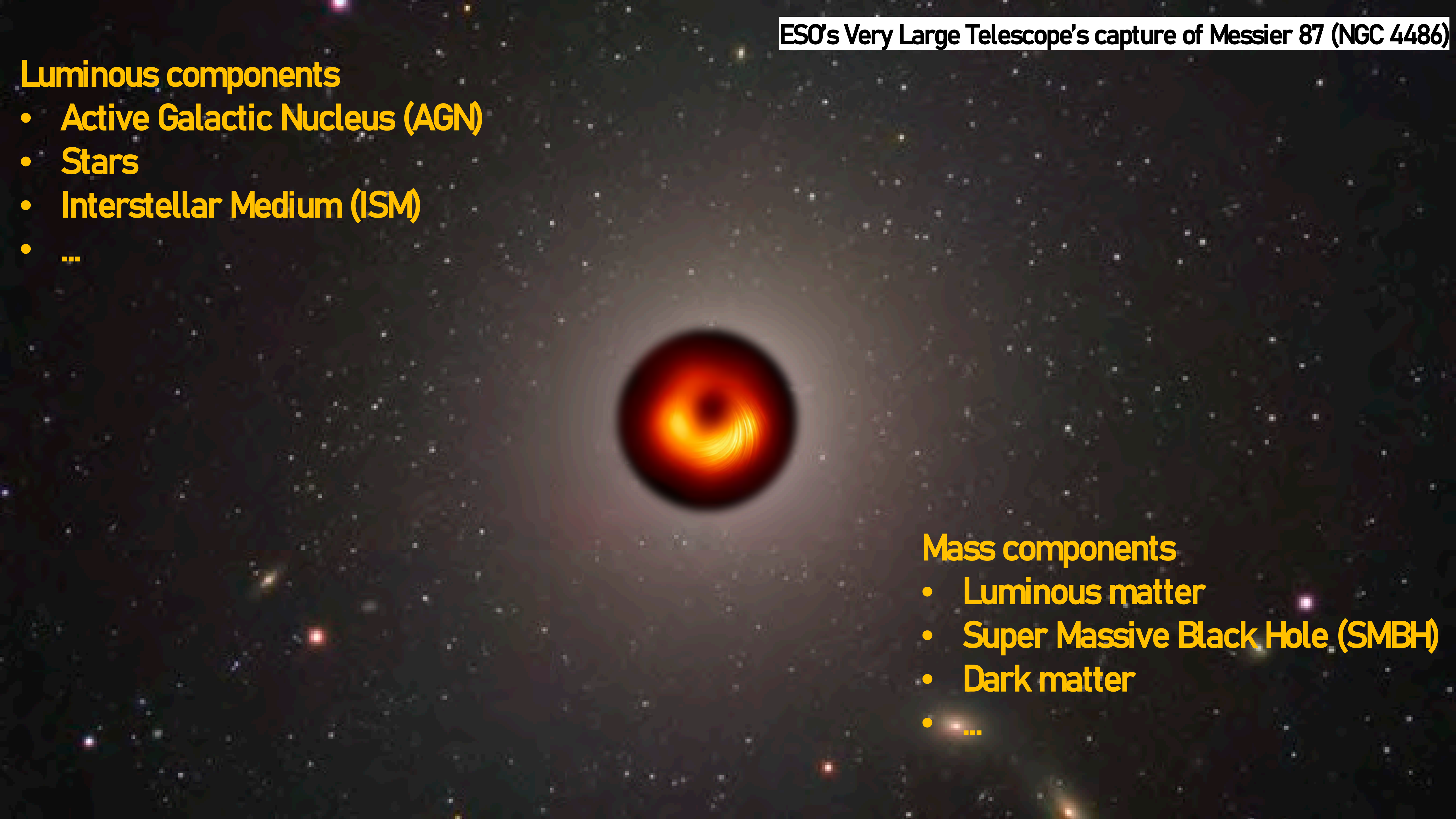
ESO's Very Large Telescope's capture of Messier 87 (NGC 4486)
Luminous components
• Active Galactic Nucleus (AGN)
• Stars
• Interstellar Medium (ISM)
• ...
Mass components
• Luminous matter
• Super Massive Black Hole (SMBH)
• Dark matter
• ...

How to get the mass distribution?

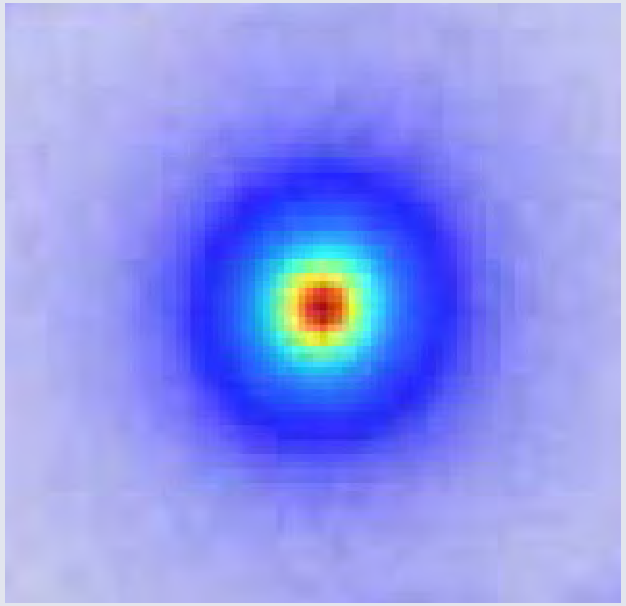

SDSS J1631+1854 (Brownstein et al. 2012)

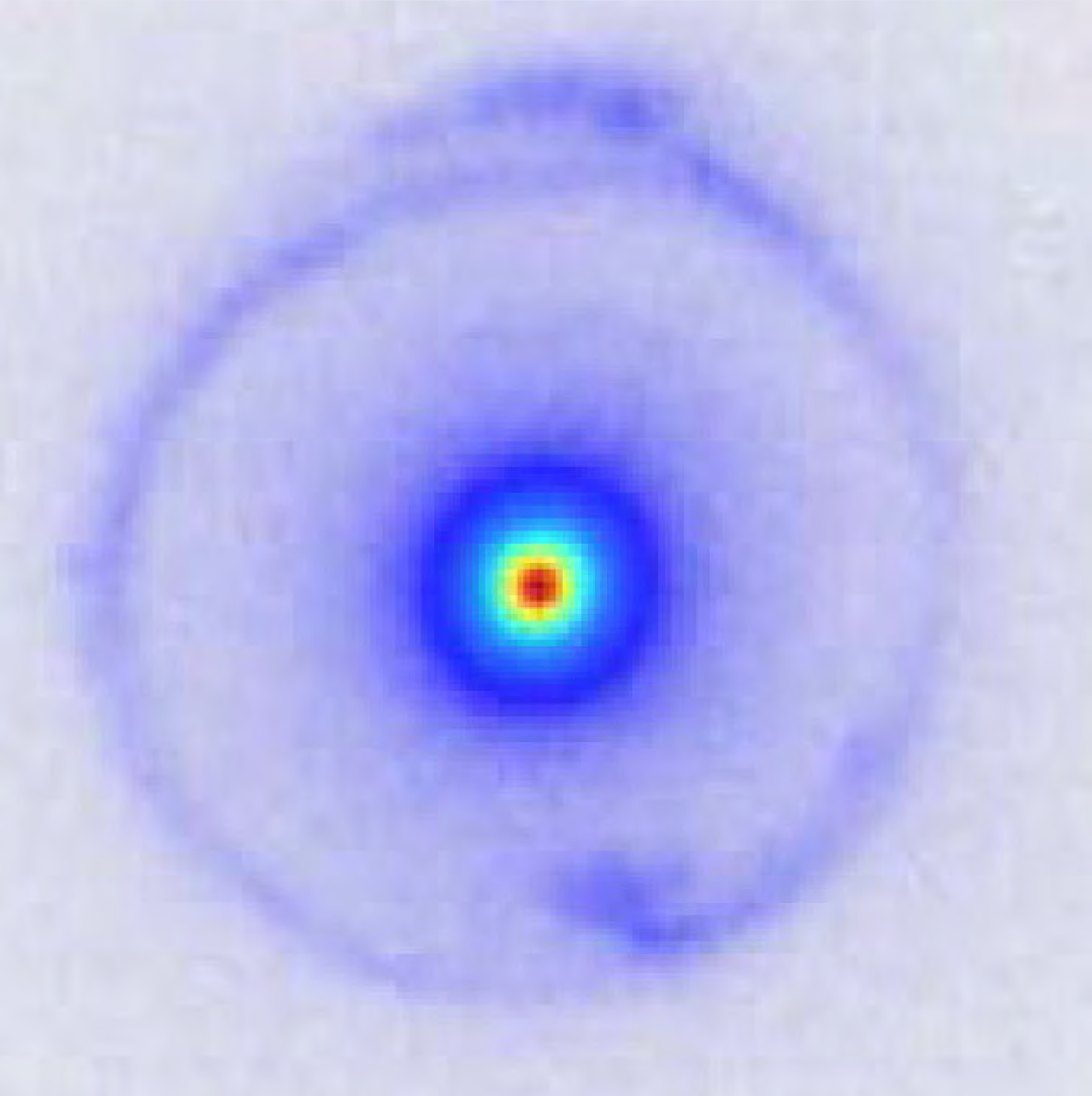

SDSS J1631+1854 (Brownstein et al. 2012)

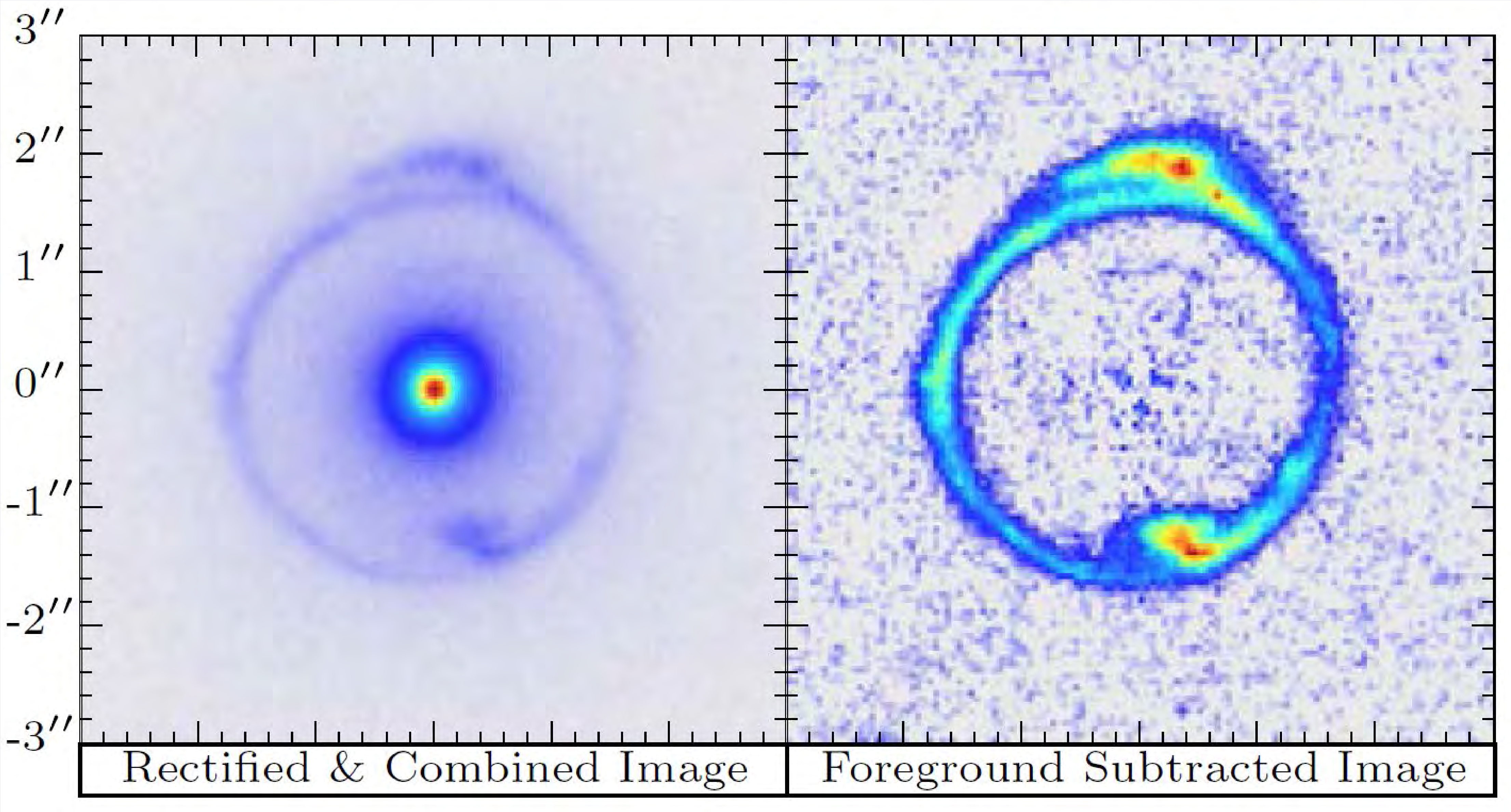

SDSS J1631+1854 (Brownstein et al. 2012)

Redshift Evolution of Lensing Galaxy Density Slopes via Model-Independent Distance Ratios

20240418

Shuaibo Geng

Collaborators: Margherita Grespan, Hareesh Thuruthipilly, Sreekanth Harikumar, and Marek Biesiada

CONTENTS

PART 1

Background

Quantities used in Astronomy

Redshift z:

$$z = \frac{f_{emi} - f_{obs}}{f_{obs}} = \frac{\lambda_{obs} - \lambda_{emi}}{\lambda_{emi}}$$

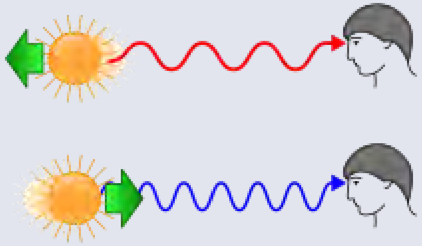

Credit: Wikipedia

Quantities used in Astronomy

Redshift z:

$$z = \frac{f_{emi} - f_{obs}}{f_{obs}} = \frac{\lambda_{obs} - \lambda_{emi}}{\lambda_{emi}}$$

$$1 + z = \frac{\lambda_{obs}}{\lambda_{emi}} = \frac{\lambda_{now}}{a \cdot \lambda_{now}} = \frac{1}{a}$$

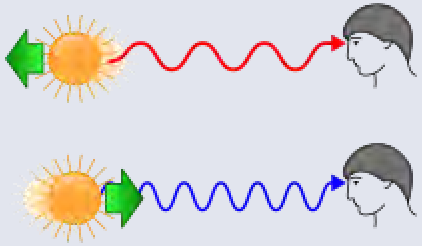

Credit: Wikipedia

a	z	t (Gyr)
1	0	13.7
0.5	1	5.95
0.21	3.76	1.70
0.1	9	0.56
0.01	99	0.017
0.001	999	0.00044

FLRW metric:

$$ds^2 = c^2dt^2 - a(t)^2[\frac{dr^2}{1-kr^2} + r^2d\theta^2 + r^2sin^2\theta d\phi^2]$$

Quantities used in Astronomy

Redshift z:

$$z = \frac{f_{emi} - f_{obs}}{f_{obs}} = \frac{\lambda_{obs} - \lambda_{emi}}{\lambda_{emi}}$$

$$1 + z = \frac{\lambda_{obs}}{\lambda_{emi}} = \frac{\lambda_{now}}{a \cdot \lambda_{now}} = \frac{1}{a}$$

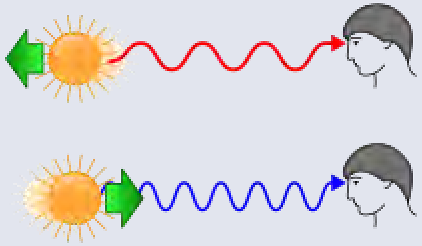

Credit: Wikipedia

a	*z*	*t* (Gyr)
1	0	13.7
0.5	1	5.95
0.21	3.76	1.70
0.1	9	0.56
0.01	99	0.017
0.001	999	0.00044

Redshift linking the distance and the time

FLRW metric:

$$ds^2 = c^2dt^2 - a(t)^2[\frac{dr^2}{1-kr^2} + r^2d\theta^2 + r^2sin^2\theta d\phi^2]$$

Quantities used in Astronomy

Redshift z:

$$z = \frac{f_{emi} - f_{obs}}{f_{obs}} = \frac{\lambda_{obs} - \lambda_{emi}}{\lambda_{emi}}$$

$$1 + z = \frac{\lambda_{obs}}{\lambda_{emi}} = \frac{\lambda_{now}}{a \cdot \lambda_{now}} = \frac{1}{a}$$

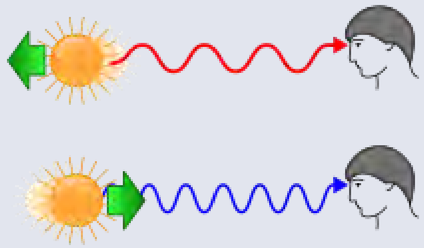

Credit: Wikipedia

a	*z*	*t* (Gyr)
1	0	13.7
0.5	1	5.95
0.21	3.76	1.70
0.1	9	0.56
0.01	99	0.017
0.001	999	0.00044

Redshift linking the distance and the time

FLRW metric:

$$ds^2 = c^2dt^2 - a(t)^2[\frac{dr^2}{1 - kr^2} + r^2d\theta^2 + r^2sin^2\theta d\phi^2]$$

Comoving distance:

$$D_c = \int_{t_e}^{t_0} \frac{cdt'}{a(t')} = \int_0^z \frac{cdz'}{H(z')} = \frac{c}{H_0}\int_0^z \frac{dz'}{E(z')}$$

$$H^2 = H_0^2\left[\Omega_r\frac{a_0^4}{a^4} + \Omega_m\frac{a_0^3}{a^3} + \Omega_k\frac{a_0^2}{a^2} + \Omega_\Lambda\right]$$

Angular diameter distance: $$D_A = \frac{1}{1+z}D_c$$

Luminosity distance: $$D_L = (1+z)D_c$$

Quantities used in Astronomy

Redshift z:

$$z = \frac{f_{emi} - f_{obs}}{f_{obs}} = \frac{\lambda_{obs} - \lambda_{emi}}{\lambda_{emi}}$$

$$1 + z = \frac{\lambda_{obs}}{\lambda_{emi}} = \frac{\lambda_{now}}{a \cdot \lambda_{now}} = \frac{1}{a}$$

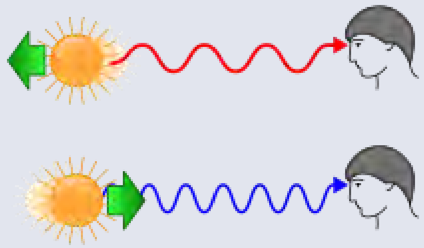

Credit: Wikipedia

a	*z*	*t* (Gyr)
1	0	13.7
0.5	1	5.95
0.21	3.76	1.70
0.1	9	0.56
0.01	99	0.017
0.001	999	0.00044

Redshift linking the distance and the time

FLRW metric:

$$ds^2 = c^2dt^2 - a(t)^2[\frac{dr^2}{1-kr^2} + r^2d\theta^2 + r^2sin^2\theta d\phi^2]$$

Comoving distance:

$$D_c = \int_{t_e}^{t_0} \frac{cdt'}{a(t')} = \int_0^z \frac{cdz'}{H(z')} = \frac{c}{H_0}\int_0^z \frac{dz'}{E(z')}$$

$$H^2 = H_0^2\left[\Omega_r\frac{a_0^4}{a^4} + \Omega_m\frac{a_0^3}{a^3} + \Omega_k\frac{a_0^2}{a^2} + \Omega_\Lambda\right]$$

Angular diameter distance: $D_A = \frac{1}{1+z}D_c$

Luminosity distance: $D_L = (1+z)D_c$

Strong Gravitational Lensing (SGL)

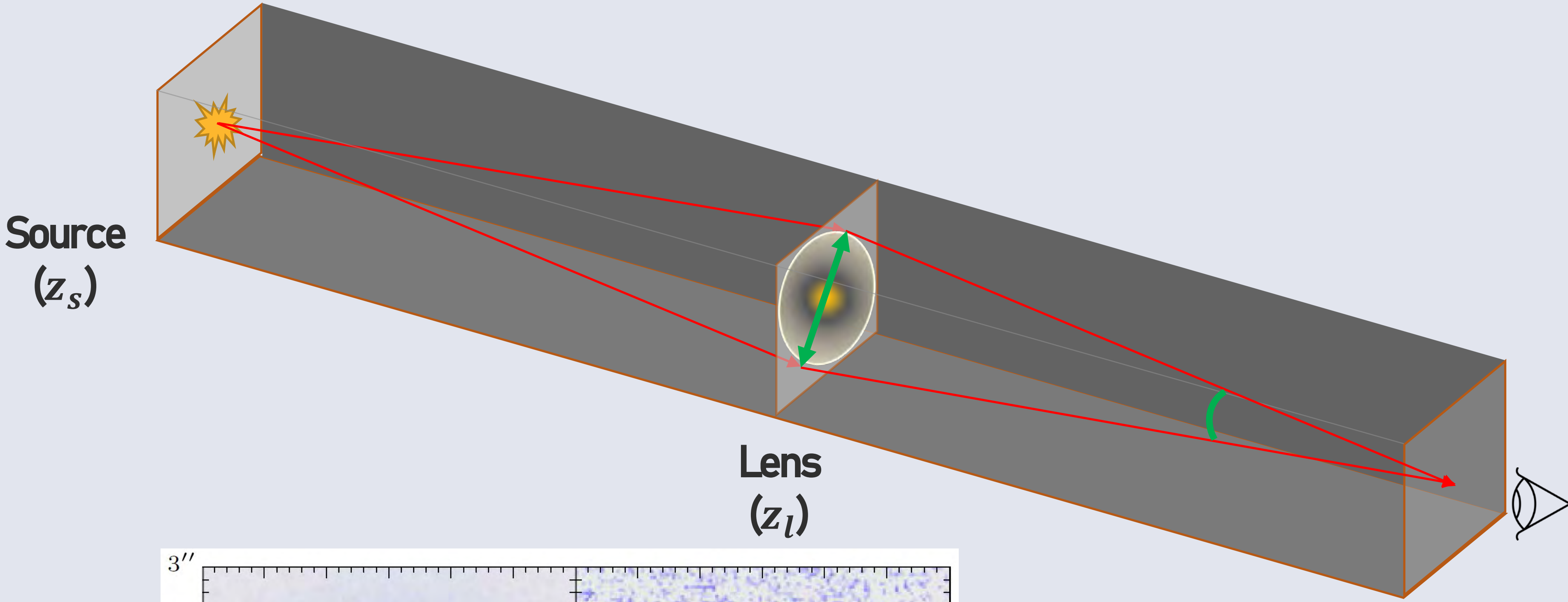

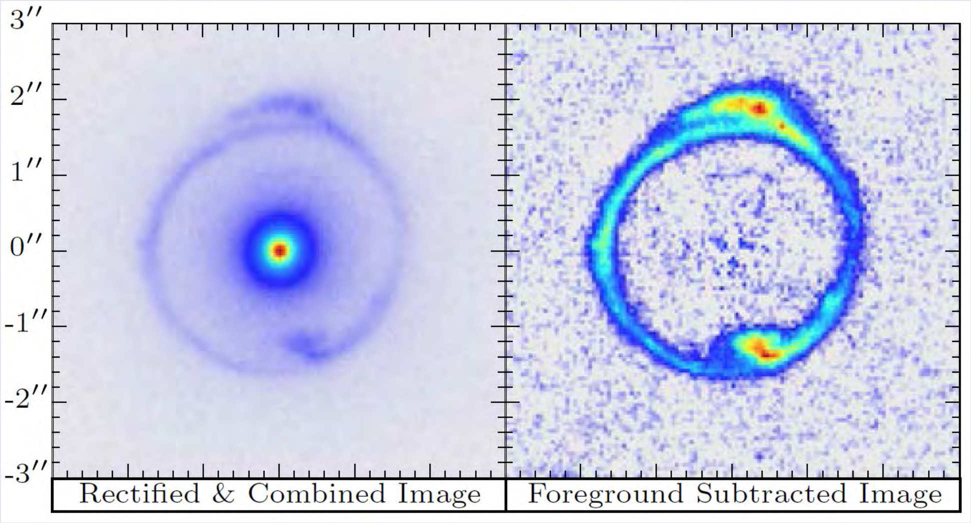

Strong Gravitational Lensing (SGL)

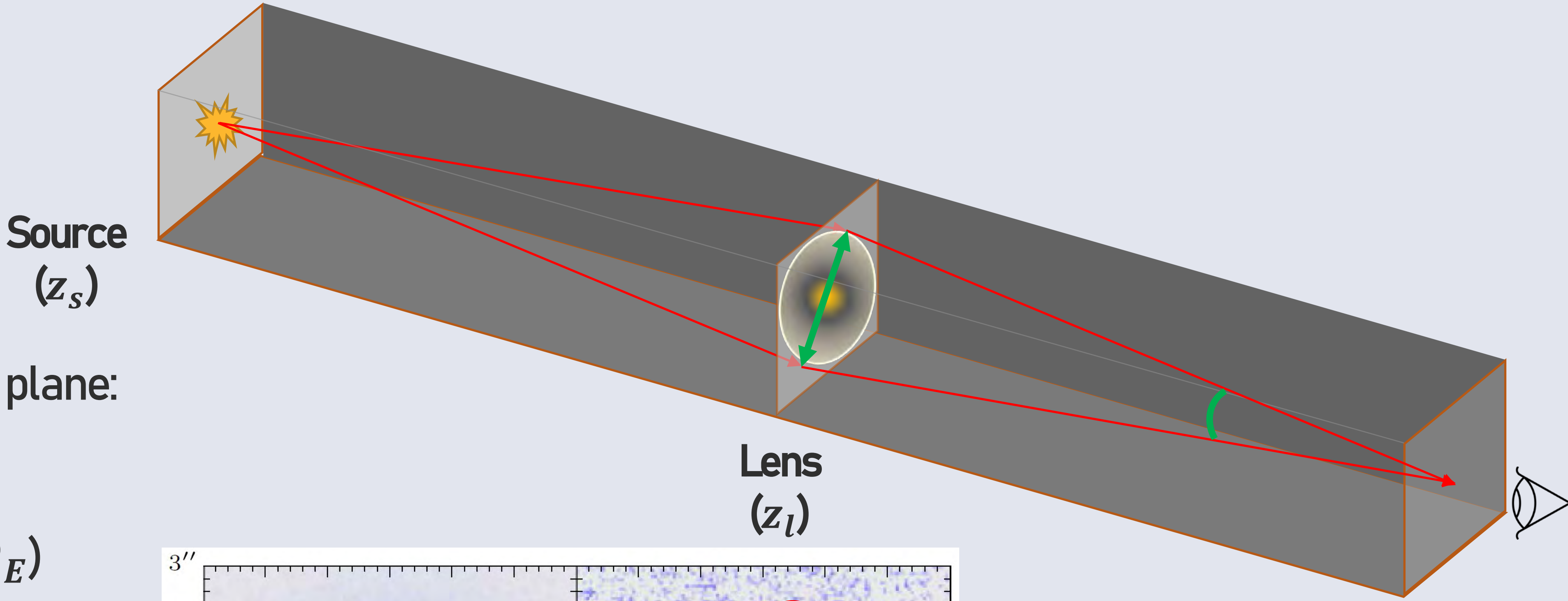

Source Images on the lens plane:

- **Source redshift (z_s)**
- **Source light distribution**
- Images' separations $(2\theta_E)$
- Flux & flux ratio of the image
- Time-delays
- ……

Lens:

- Lens redshift (z_l)
- Velocity dispersion (σ)
- ……

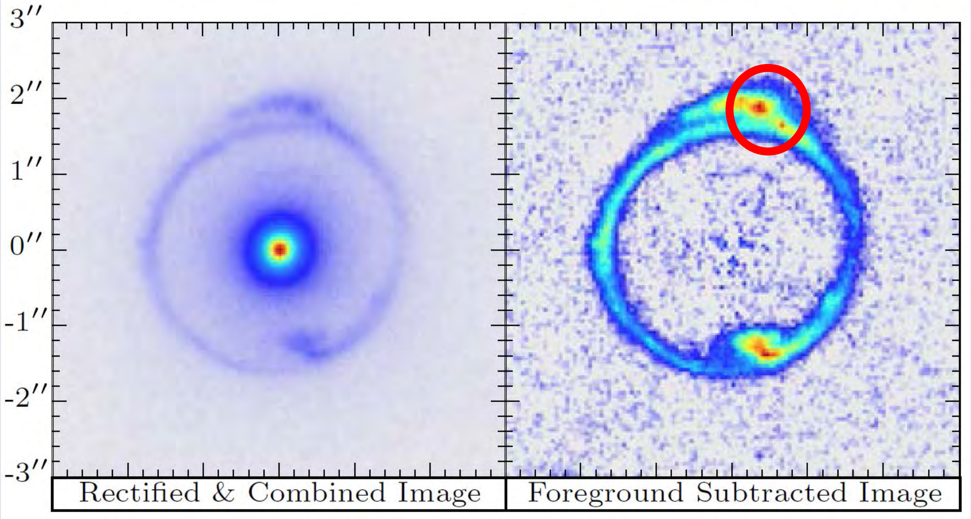

Strong Gravitational Lensing (SGL)

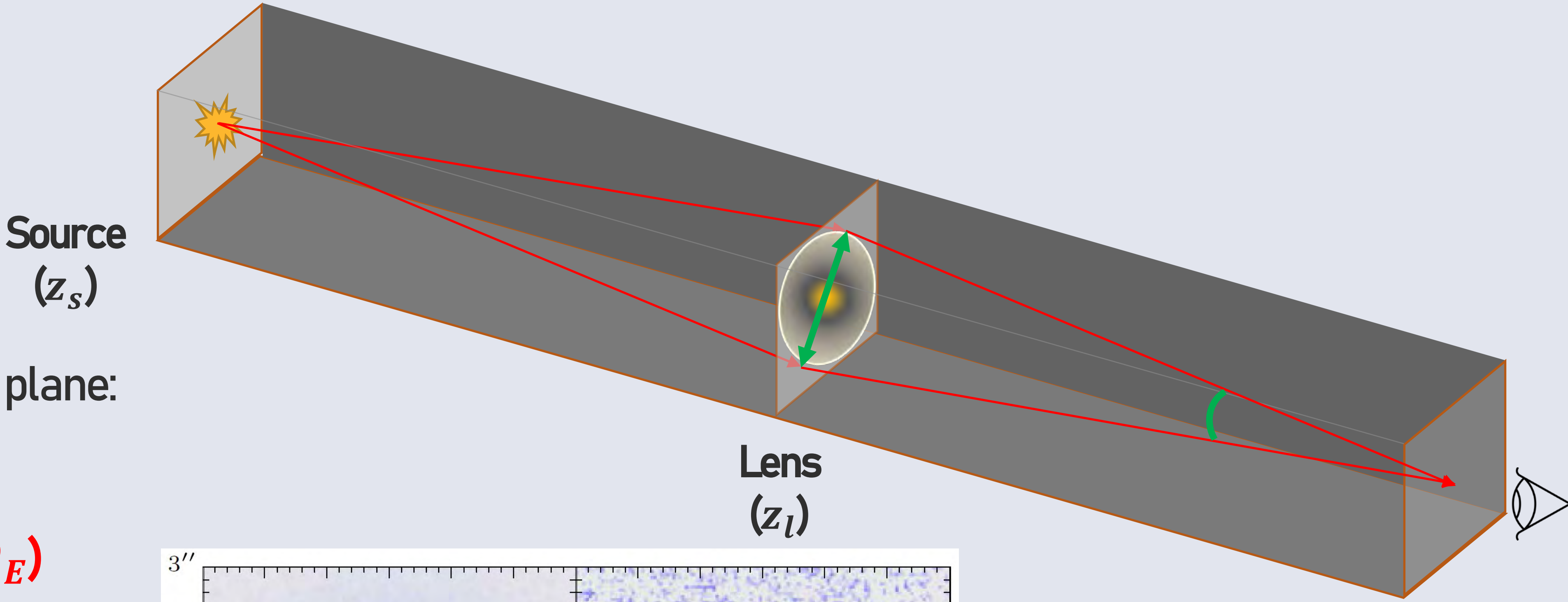

Source Images on the lens plane:

- Source redshift (z_s)
- Source light distribution
- **Images' separations ($2\theta_E$)**
- **Flux & flux ratio of the image**
- Time-delays
- ......

Lens:

- Lens redshift (z_l)
- Velocity dispersion (σ)
- ......

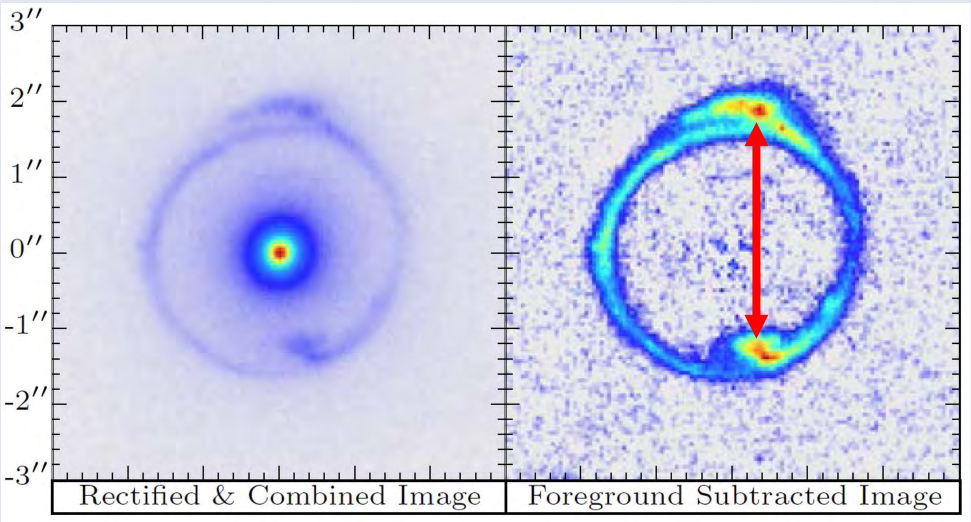

Strong Gravitational Lensing (SGL)

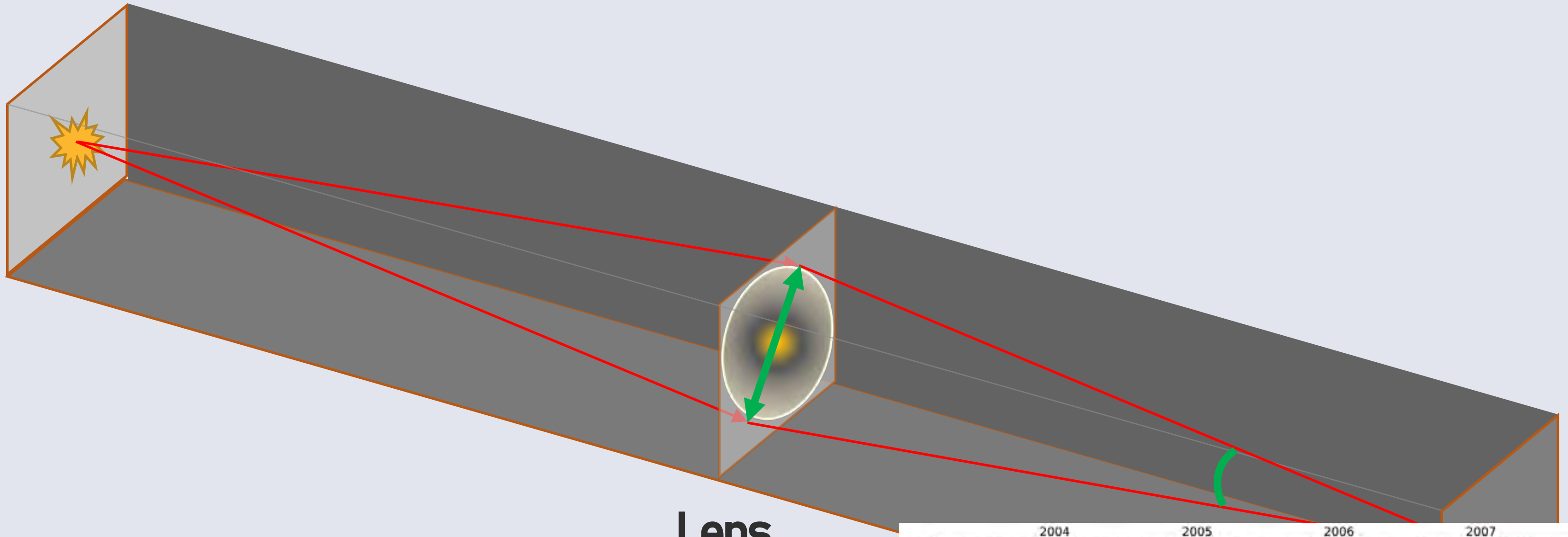

Source
(z_s)

Lens
(z_l)

Source Images on the lens plane:
- Source redshift (z_s)
- Source light distribution
- Images' separations (θ_E)
- Flux & flux ratio of the image
- **Time-delays**
- ……

Lens:
- Lens redshift (z_l)
- Velocity dispersion (σ)
- ……

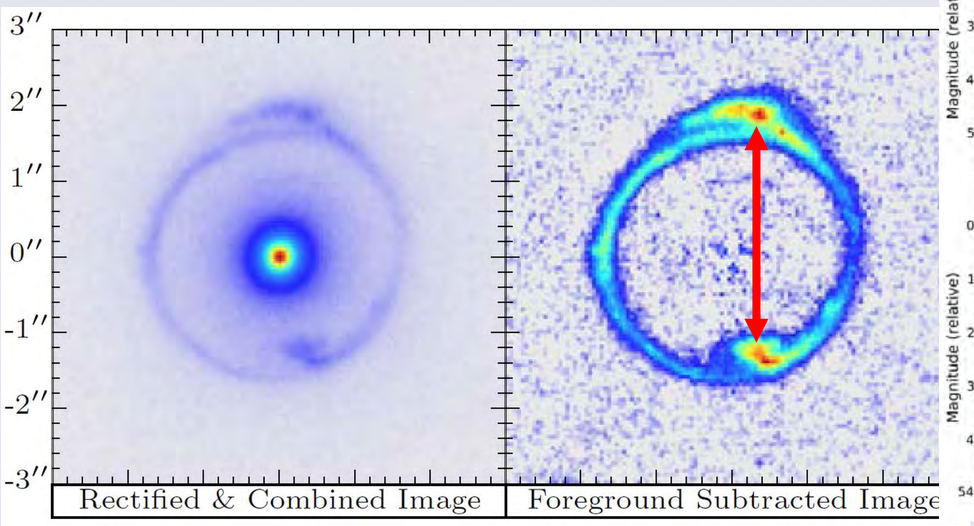

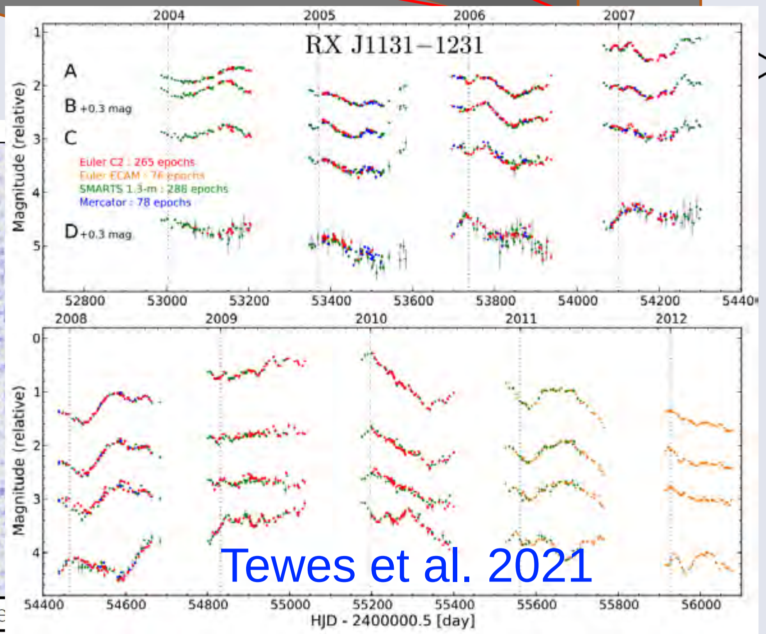

Strong Gravitational Lensing (SGL)

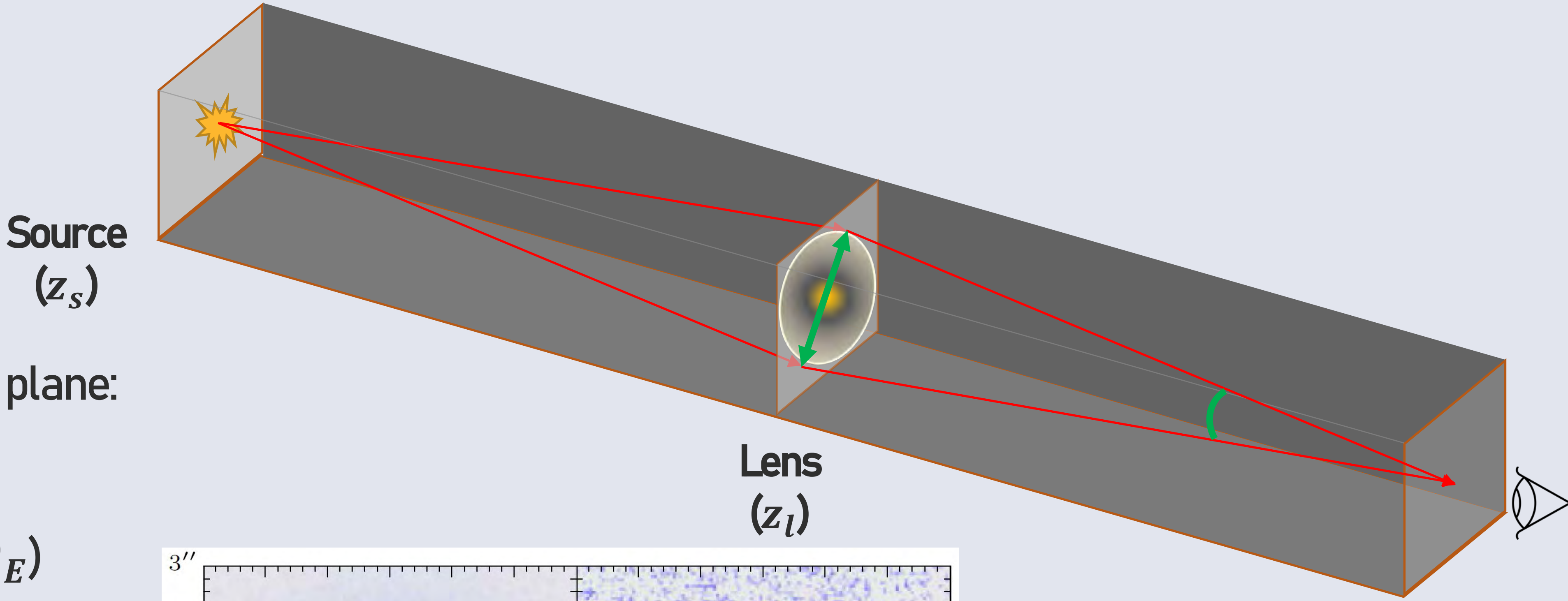

Source Images on the lens plane:

- Source redshift (z_s)
- Source light distribution
- Images' separations ($2\theta_E$)
- Flux & flux ratio of the image
- Time-delays
- ……

Lens:

- **Lens redshift (z_l)**
- **Velocity dispersion (σ)**
- ……

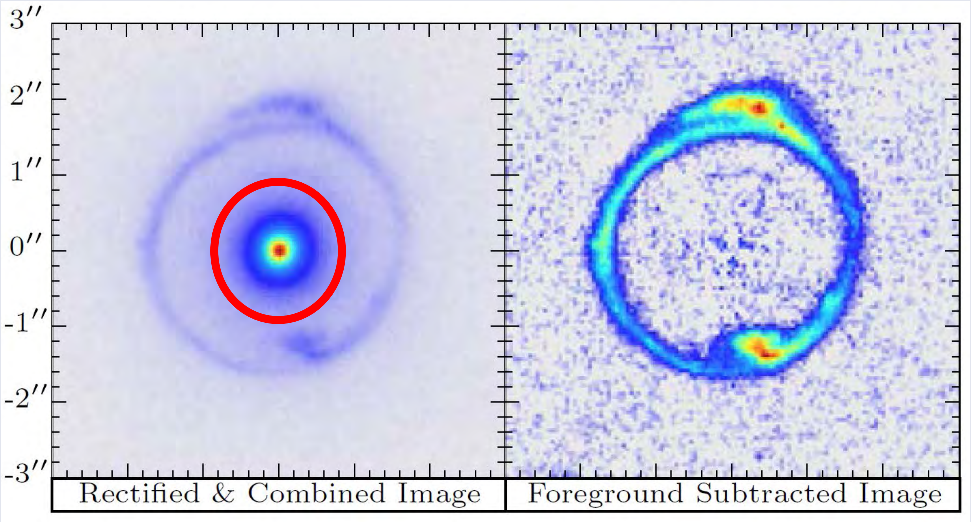

Strong Gravitational Lensing (SGL)

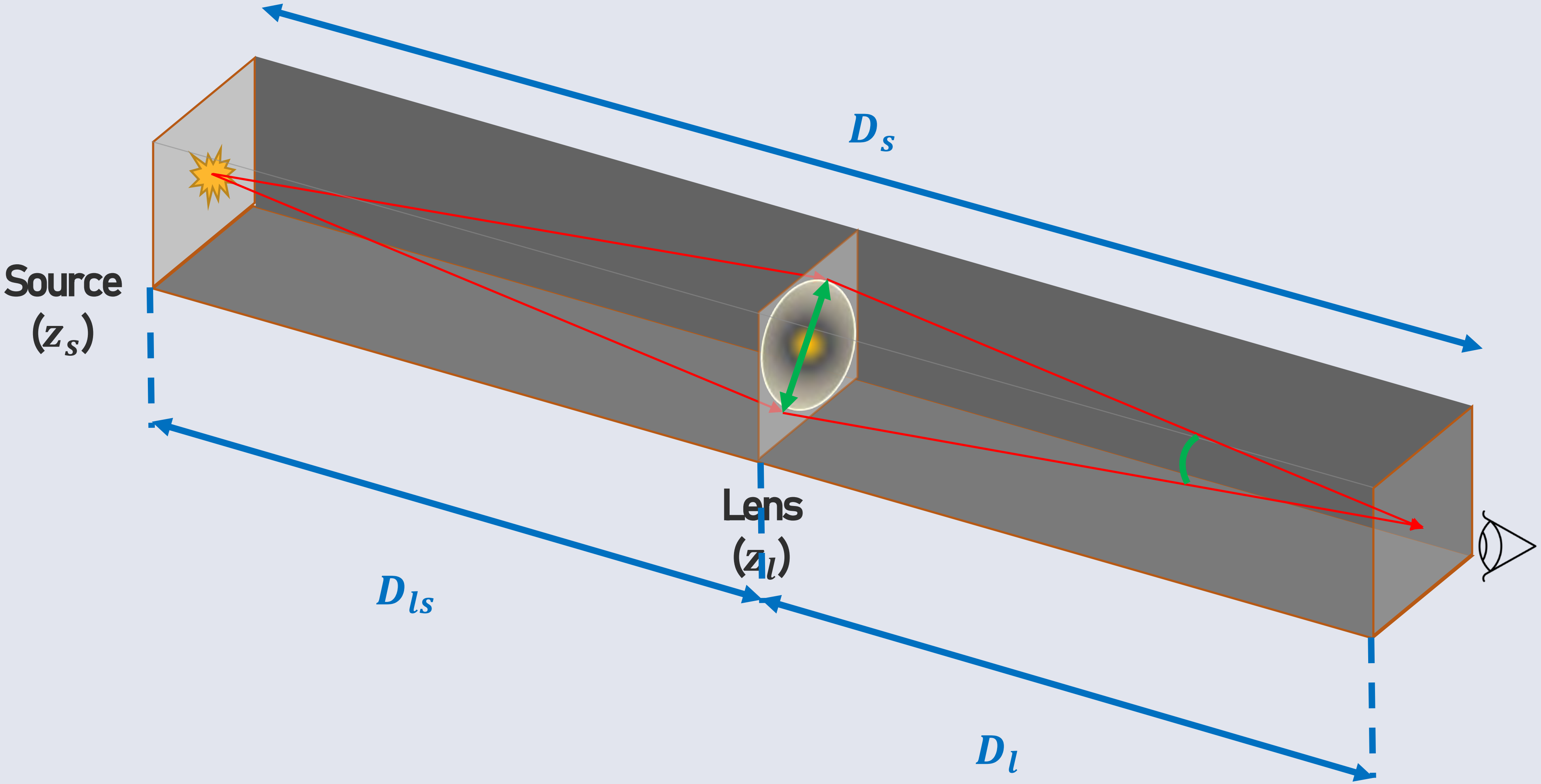

Strong Gravitational Lensing (SGL)

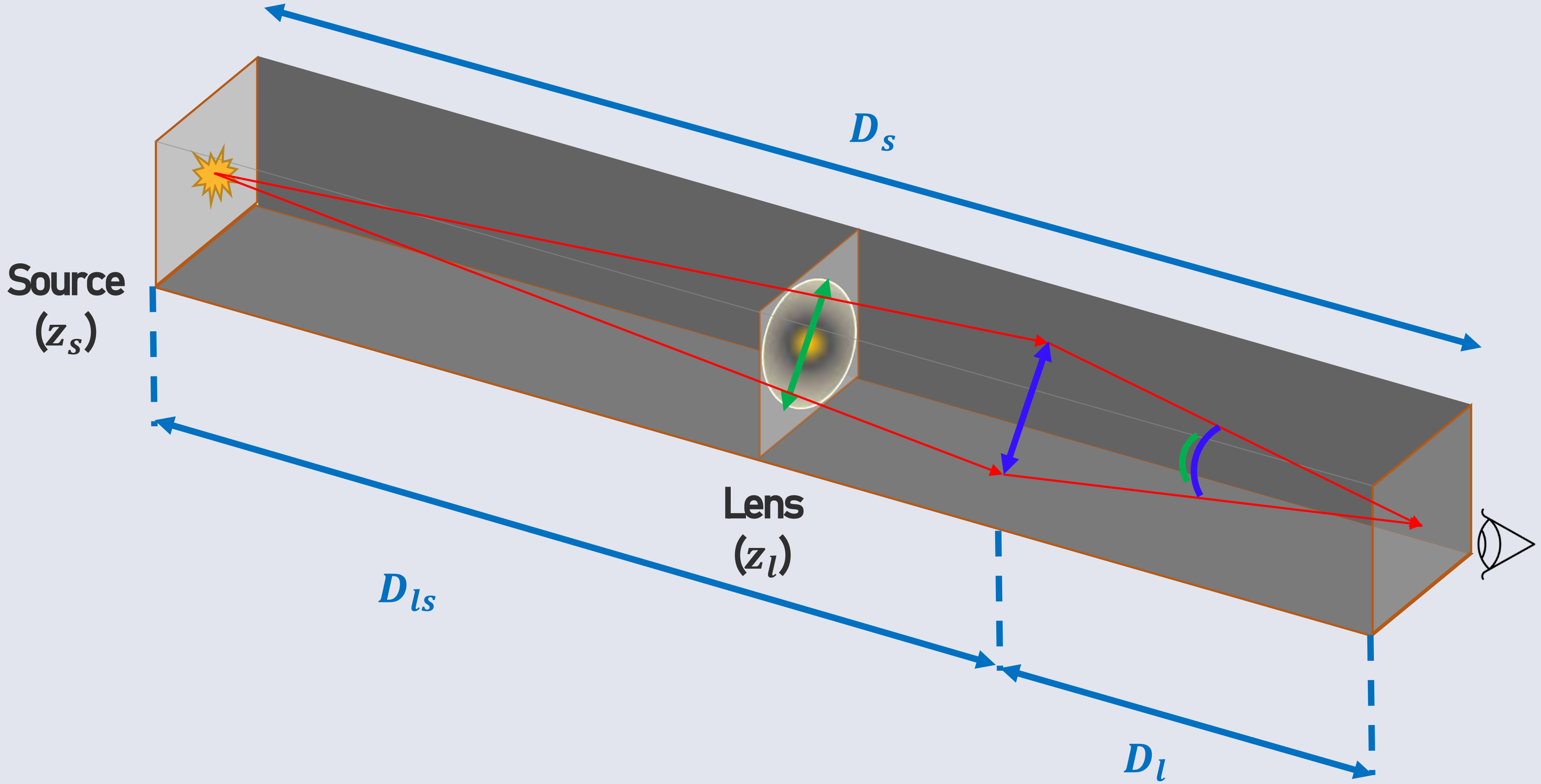

Strong Gravitational Lensing (SGL)

Einstein radius (θ_E) in Singular isothermal sphere model

$$\theta_E = 4\pi \frac{\sigma_{SIS}^2}{c^2} \frac{D_{ls}}{D_s}$$

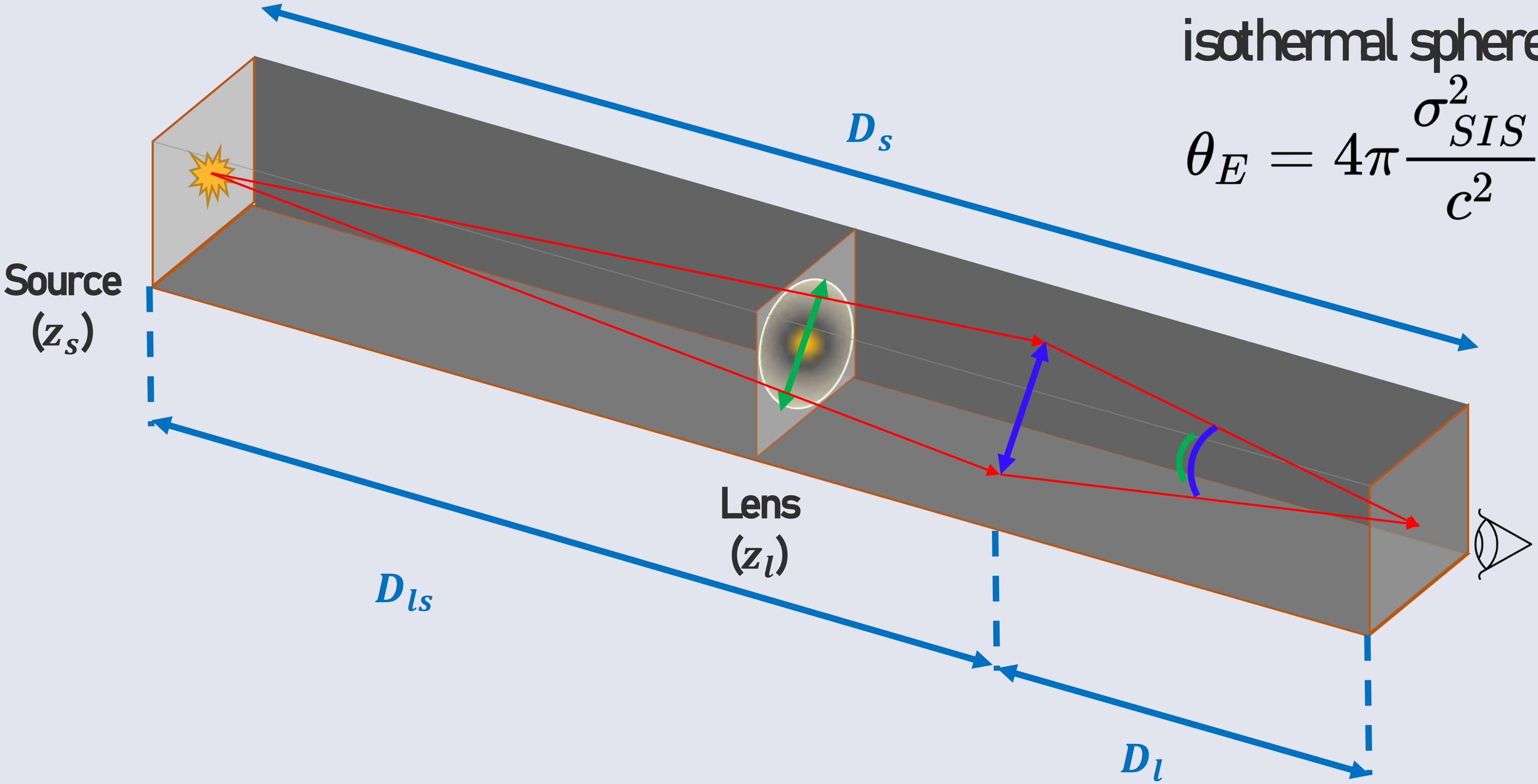

Strong Gravitational Lensing (SGL)

Einstein radius (θ_E) in Singular isothermal sphere model

$$\theta_E = 4\pi \frac{\sigma_{SIS}^2}{c^2} \frac{D_{ls}}{D_s}$$

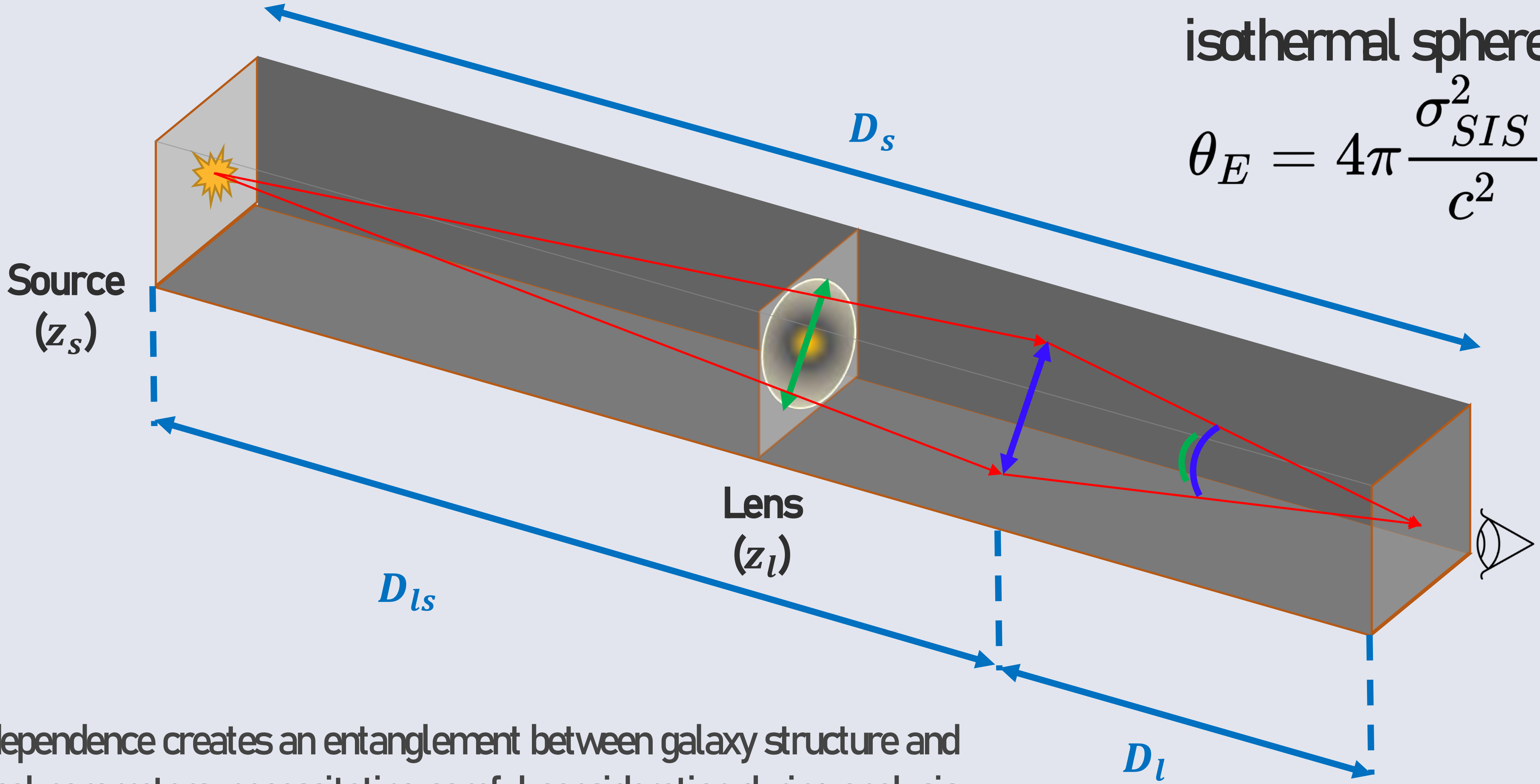

This interdependence creates an entanglement between galaxy structure and cosmological parameters, necessitating careful consideration during analysis.

SGL Applications on Cosmology

Di Valentino et al. 2021

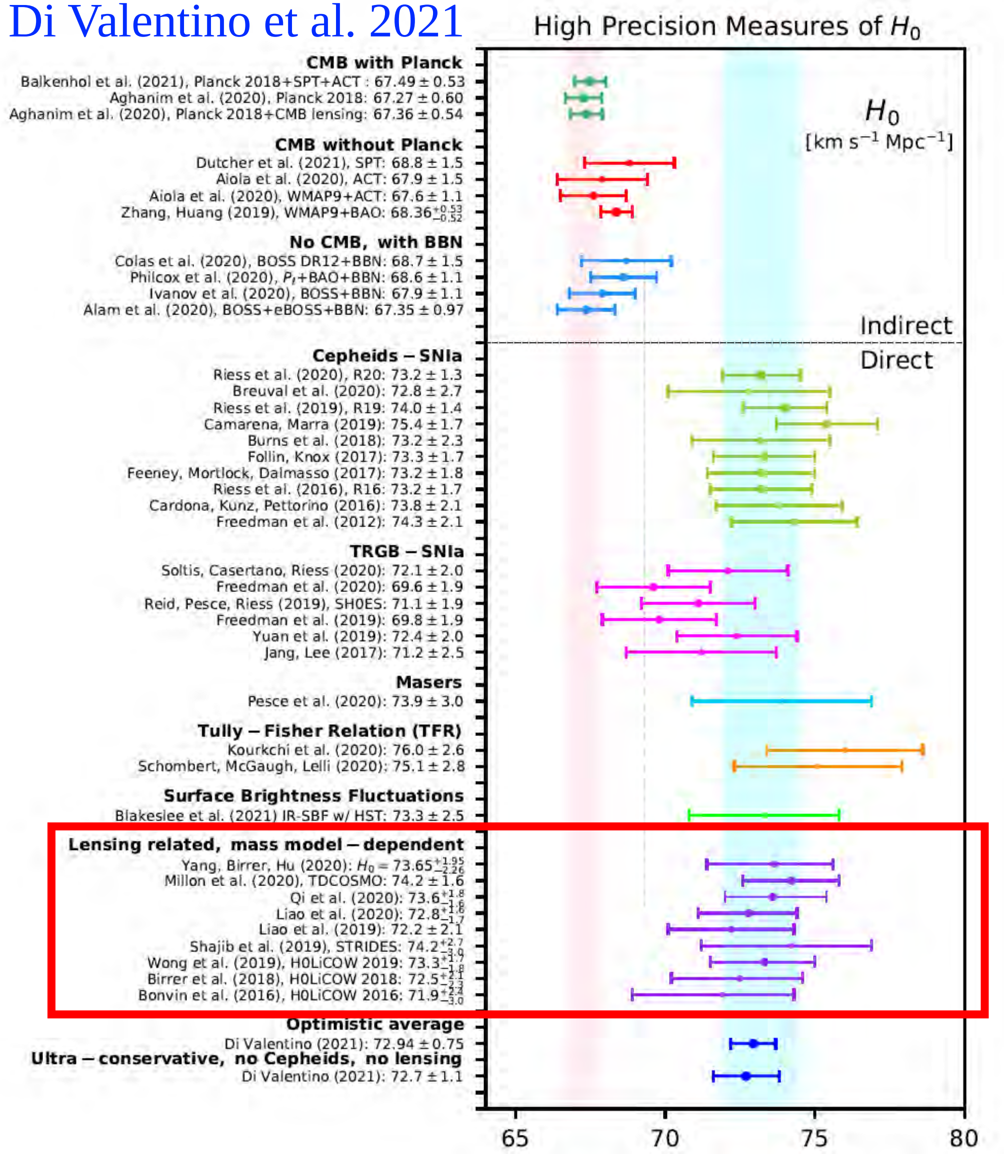

SGL Applications on Cosmology

Di Valentino et al. 2021

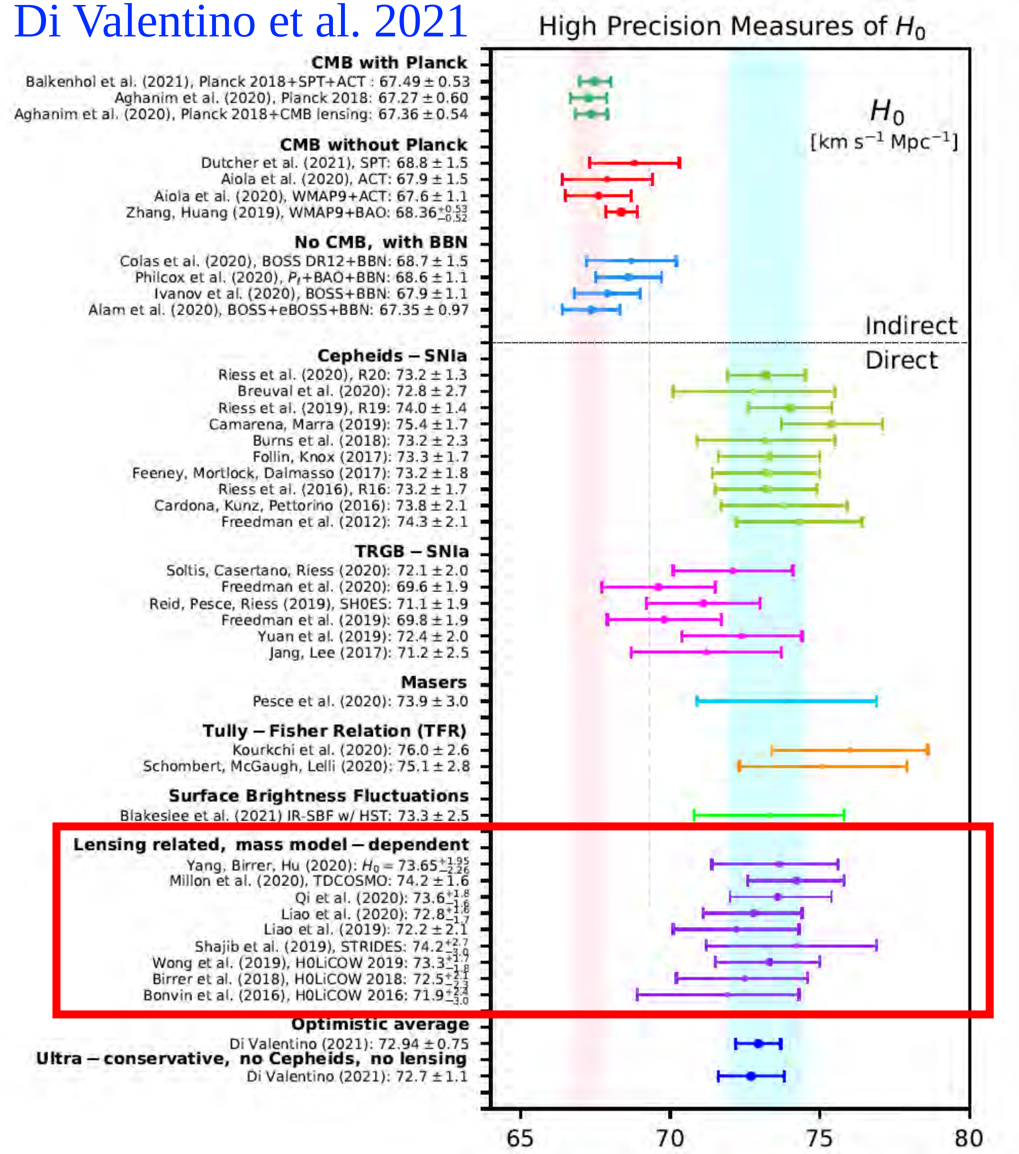

Li et al. 2024

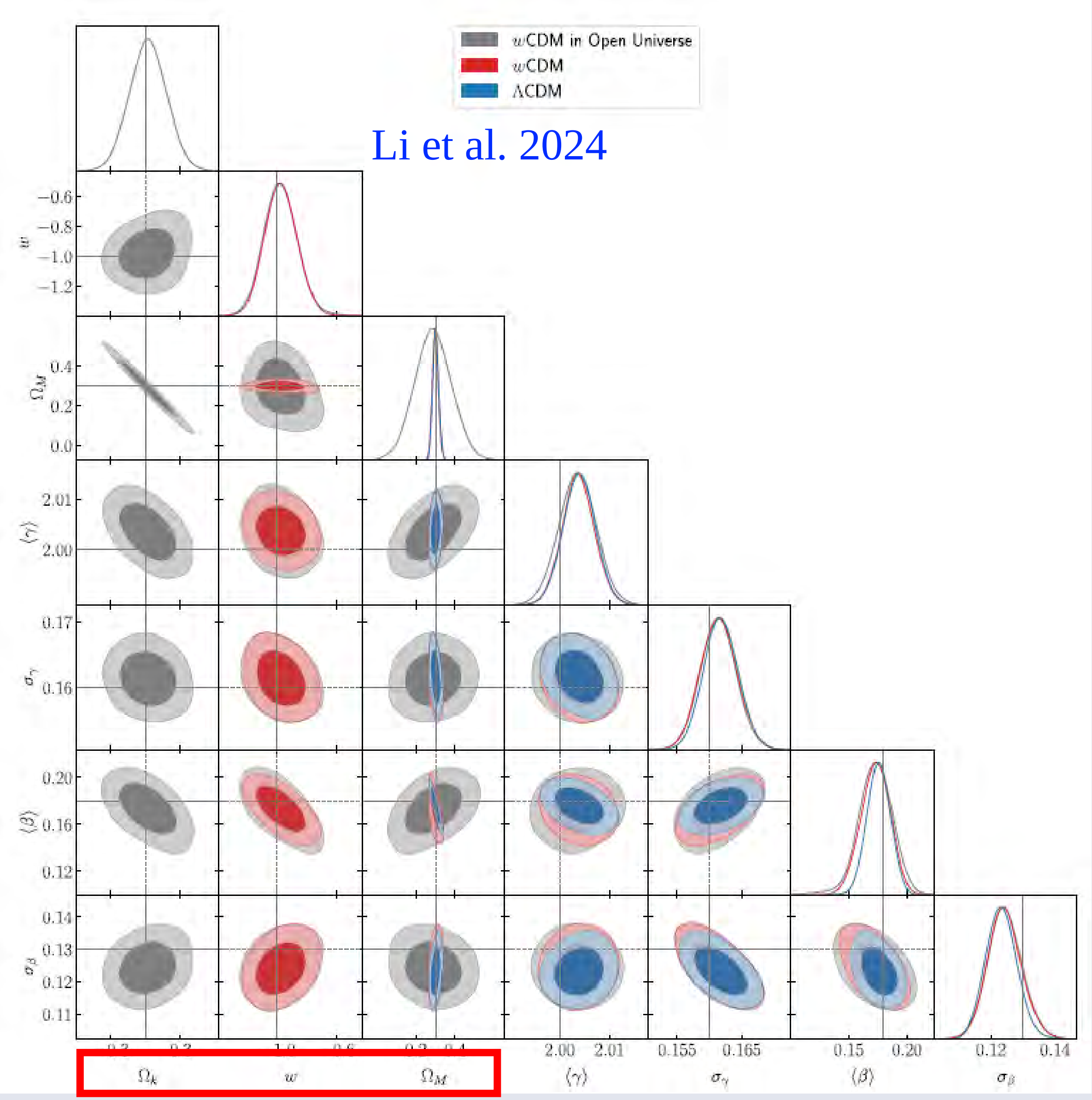

PART 2

Lens model

Spherically symmetric power-law model (SPL)

Lens Model

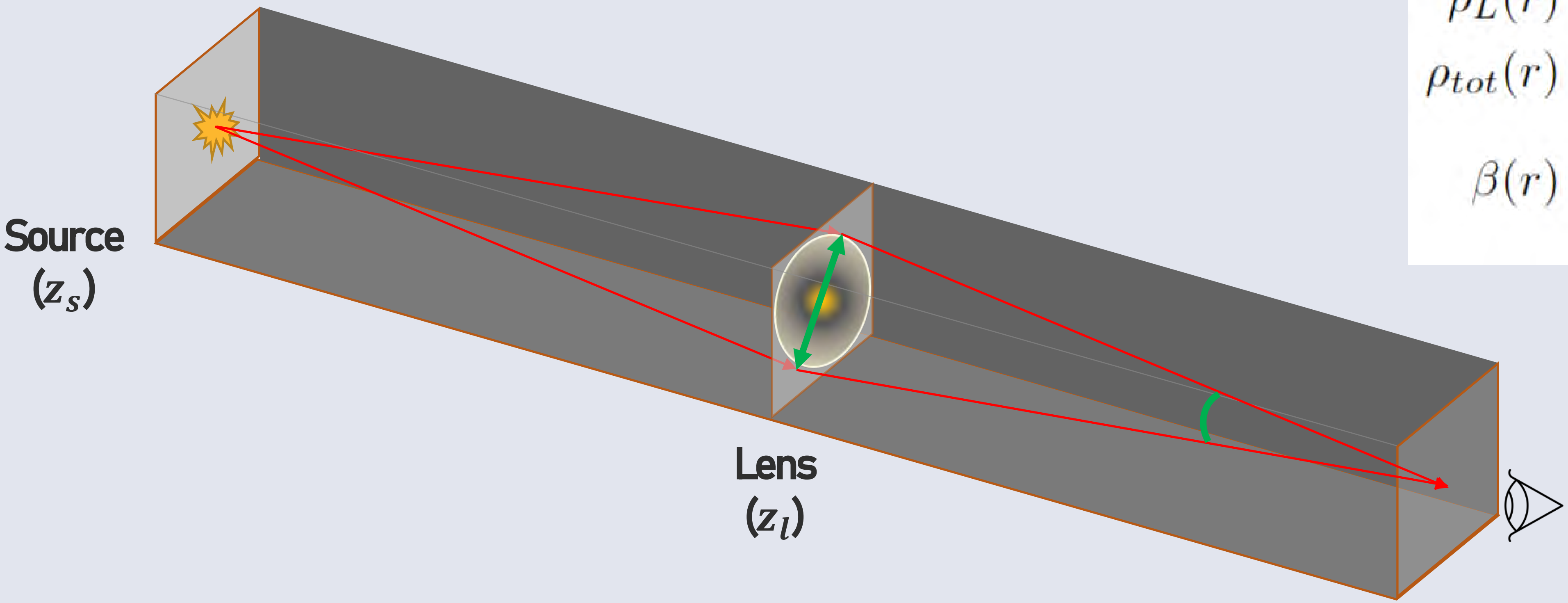

$$\rho_L(r) = \rho_L r^{-\delta}$$

$$\rho_{tot}(r) = \rho_{tot} r^{-\gamma}$$

$$\beta(r) = 1 - \frac{\langle \sigma_\theta^2 \rangle}{\langle \sigma_r^2 \rangle},$$

Spherically symmetric power-law model (SPL)

Lens Model

$$\rho_L(r) = \rho_L r^{-\delta}$$

$$\rho_{tot}(r) = \rho_{tot} r^{-\gamma}$$

$$\beta(r) = 1 - \frac{\langle \sigma_\theta^2 \rangle}{\langle \sigma_r^2 \rangle},$$

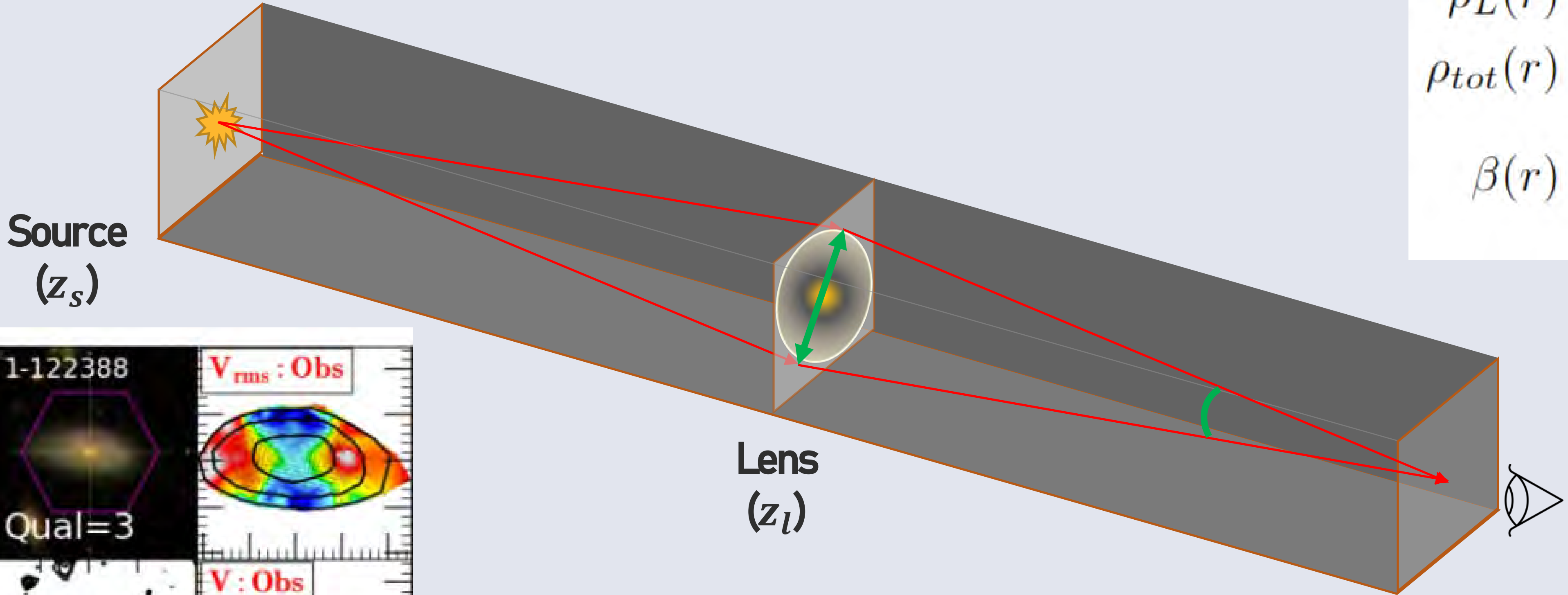

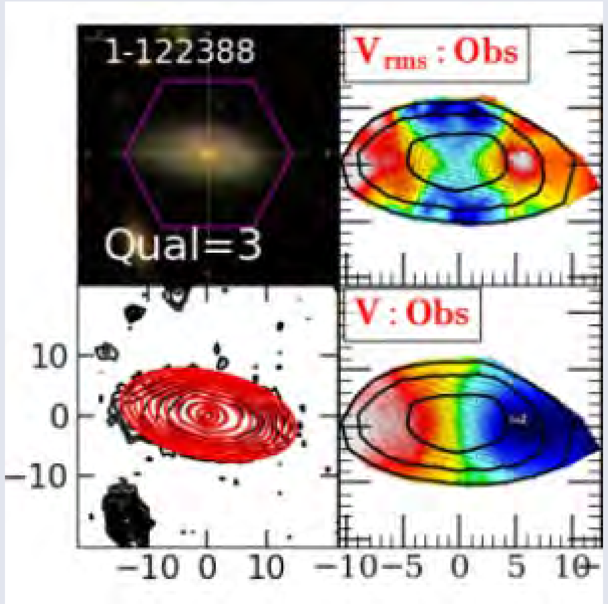

Spherically symmetric power-law model (SPL)

Lens Model

$$\rho_L(r) = \rho_L r^{-\delta}$$

$$\rho_{tot}(r) = \rho_{tot} r^{-\gamma}$$

$$\beta(r) = 1 - \frac{\langle \sigma_\theta^2 \rangle}{\langle \sigma_r^2 \rangle},$$

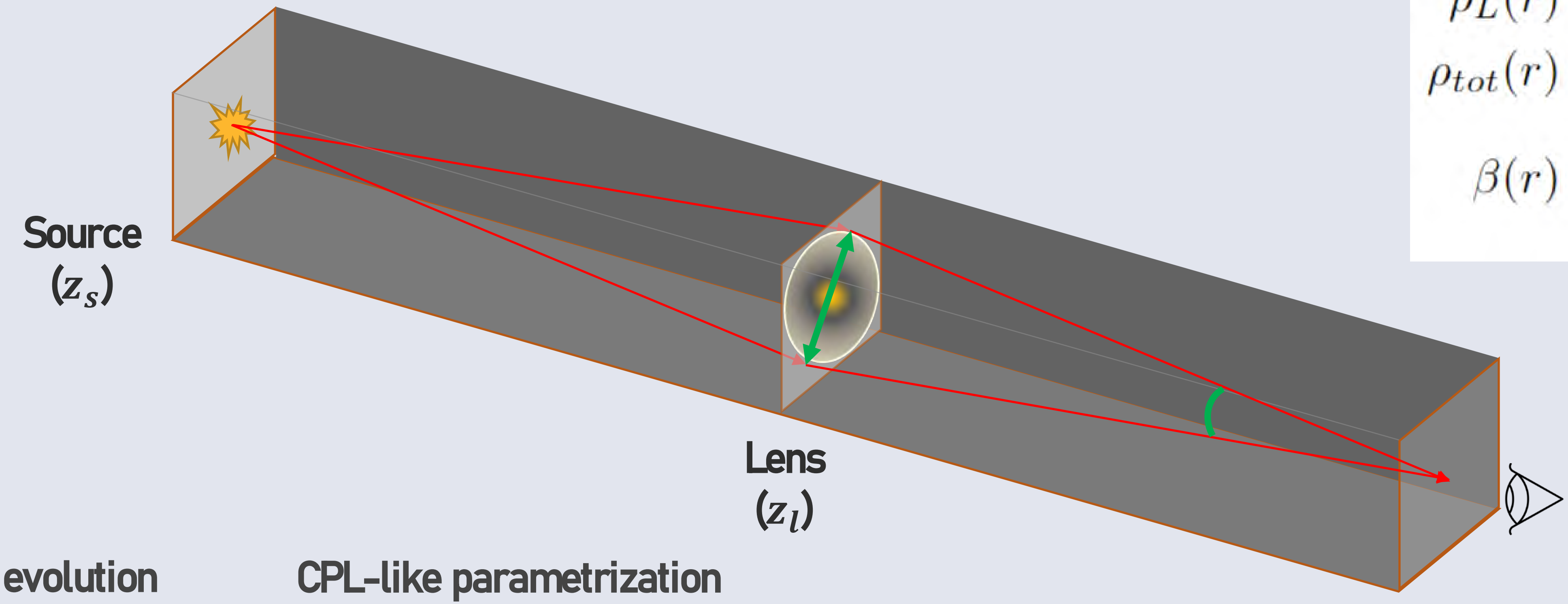

Linear evolution

$$\gamma = \gamma_0 + z_l \times \gamma_s$$

$$\delta = \delta_0 + z_l \times \delta_s$$

CPL-like parametrization

$$\gamma = \gamma_0 + \frac{z_l}{1+z_l} \times \gamma_s$$

$$\delta = \delta_0 + \frac{z_l}{1+z_l} \times \delta_s$$

Spherically symmetric power-law model (SPL)

Lens Model

$$\rho_L(r) = \rho_L r^{-\delta}$$

$$\rho_{tot}(r) = \rho_{tot} r^{-\gamma}$$

$$\beta(r) = 1 - \frac{\langle \sigma_\theta^2 \rangle}{\langle \sigma_r^2 \rangle},$$

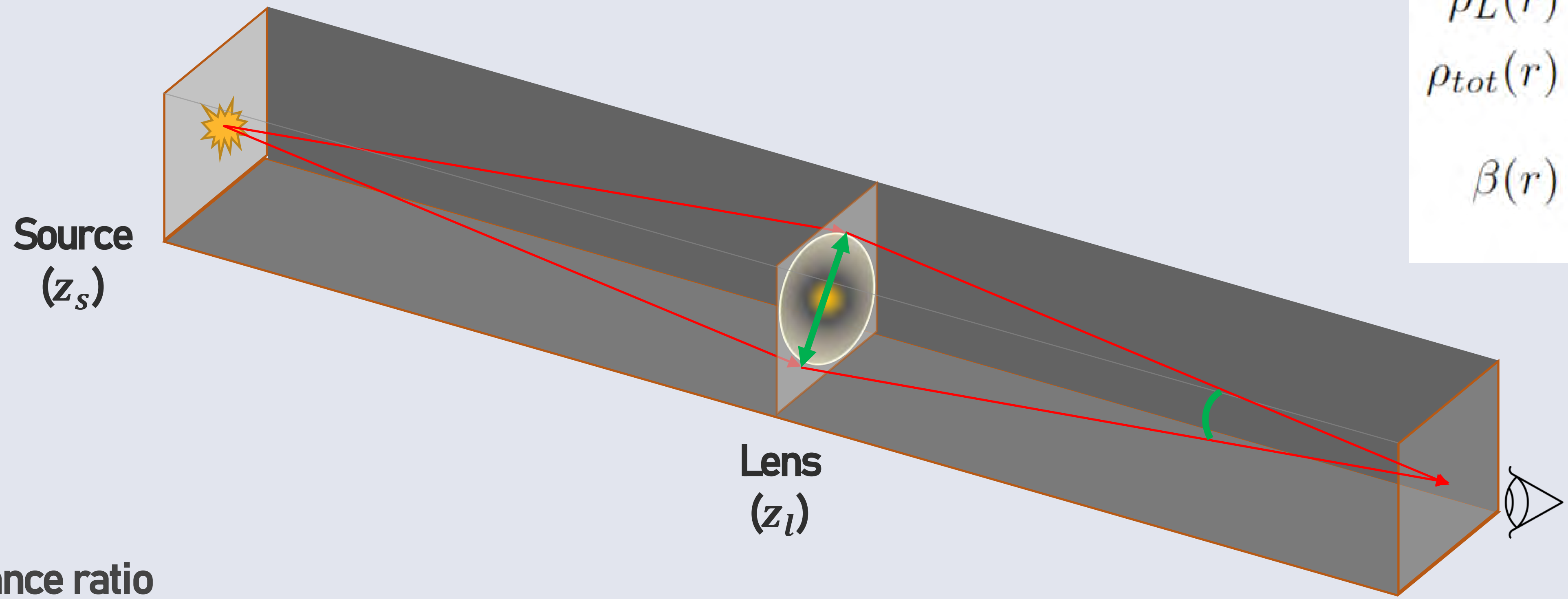

Distance ratio

$$\frac{D_{ls}}{D_s} = \frac{c^2}{4\pi} \frac{\theta_E}{\sigma_{ap}^2} \left(\frac{\theta_E}{\theta_{ap}} \right)^{\gamma - 2} f^{-1}(\gamma, \delta, \beta)$$

Spherically symmetric power-law model (SPL)

Power-law model works well inside the Einstein radius.

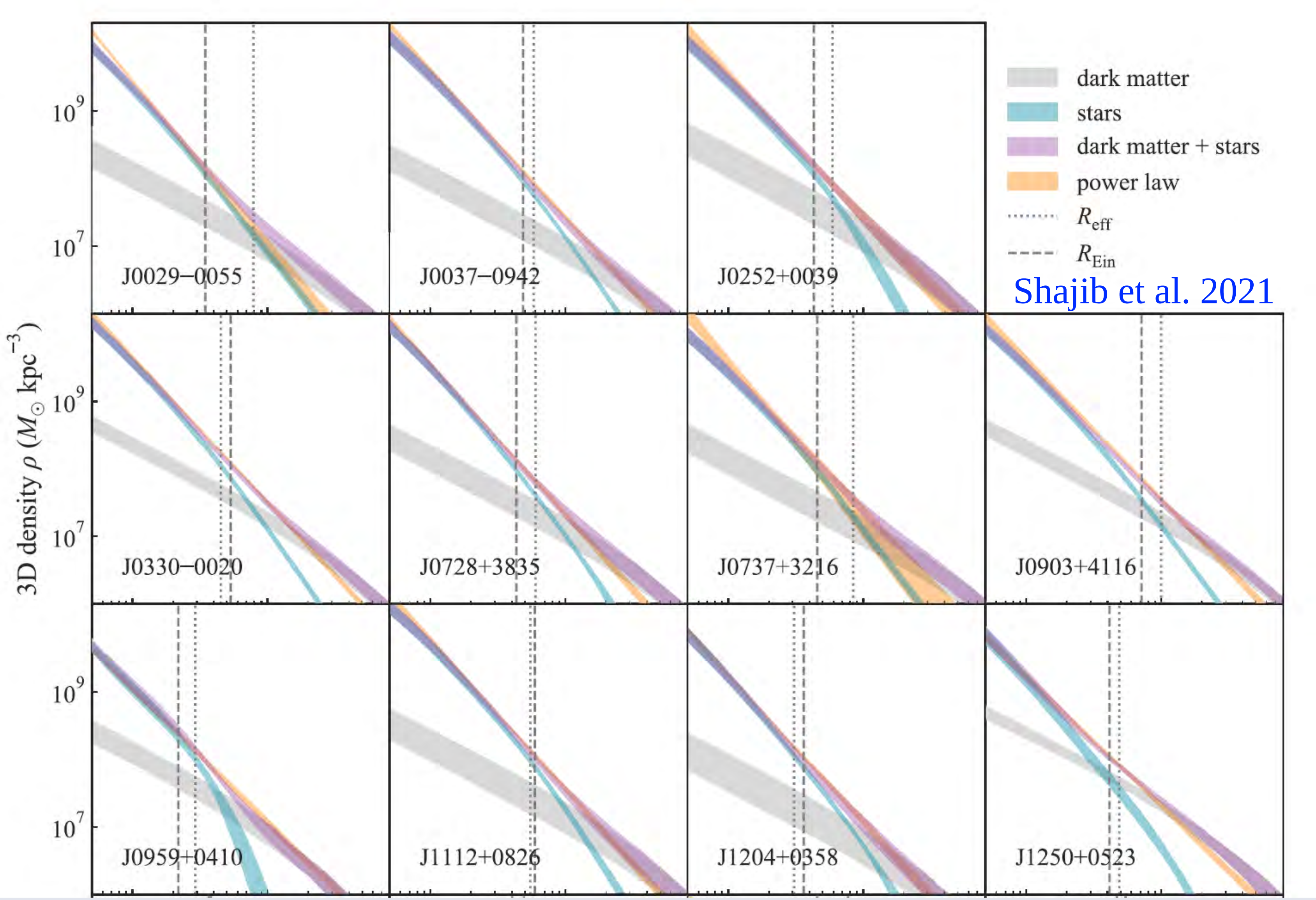

SPL model Applications

Application	Work	Authors	
Galaxy evolution	Exploring the Possible Evolution of the Mass Density Power-law Index of Strong Gravitational Lenses with a Model-independent Method	Hu 2023	Dali University
Cosmology constraints, FLRW metric, cosmic curvature	Cosmology from large populations of galaxy-galaxy strong gravitational lenses	Li et al. 2024	University of Portsmouth
	Constraining cosmological and galaxy parameters using strong gravitational lensing systems	Kumar et al 2021	University of Delhi
	Cosmological Parameter Estimation Using Current and Future Observations of Strong Gravitational Lensing	Qi et al 2022	Northeastern University
	Constraining the Spatial Curvature of the Local Universe with Deep Learning	Liu et al 2023	Mianyang Teachers' College
	Cosmological model-independent measurement of cosmic curvature using distance sum rule with the help of gravitational waves	Wang et al 2022	Northeastern University
	Cosmological Model-independent Constraints on Spatial Curvature from Strong Gravitational Lensing and SN Ia Observations	Wang et al 2020	Northeastern University
	Direct test of the FLRW metric from strongly lensed gravitational wave observations	Cao et al 2019	Beijing Normal University
	Assessing the effect of lens mass model in cosmological application with updated galaxy-scale strong gravitational lensing sample	Chen et al 2019	National Astronomical Observatories
GR test & Post-Newtonian parameter	Probing a scale dependent gravitational slip with galaxy strong lensing systems	Guerrini & Mortsell 2024	Ecole Polytechnique, Palaiseau,
	Direct Tests of General Relativity under Screening Effect with Galaxy-scale Strong Lensing Systems	Lian et al 2022	Beijing Normal University
	Direct Estimate of the Post-Newtonian Parameter and Cosmic Curvature from Galaxy-scale Strong Gravitational Lensing	Wei et al 2022	Purple Mountain Observatory
	Galaxy-scale Test of General Relativity with Strong Gravitational Lensing	Liu et al 2022	Northeastern University
Cosmic distance duality relation	Deep learning method for testing the cosmic distance duality relation	Li et al 2023	Chongqing University
	On the cosmic distance duality relation and strong gravitational lens power law density profile	Lima et al 2021	Federal University of Rio Grande do Norte
	Test of the cosmic distance duality relation for arbitrary spatial curvature	Qin et al 2021	Beijing Normal University
Dark matter	A new way to test the WIMP dark matter models	Cheng et al 2021	Chongqing University of Posts and Telecommunications
	Probing the dark matter density evolution law with large scale structures	Bora et al 2021	Indian Institute of Technology
Speed of light	Constraining a possible time-variation of the speed of light along with the fine-structure constant using strong gravitational lensing and Type Ia supernovae observations	Colaco et al 2022	Federal University of Rio Grande do Norte
	Consistency testing for invariance of the speed of light at different redshifts: the newest results from strong lensing and Type Ia supernovae observations	Liu et al 2021	Beijing Normal University
Gas depletion factor evolution	A test of the evolution of gas depletion factor in galaxy clusters using strong gravitational lensing systems	Holanda 2022	Federal University of Rio Grande do Sul

Why study density slopes of early-type galaxies and their redshift evolution?

Why study density slopes of early-type galaxies and their redshift evolution?

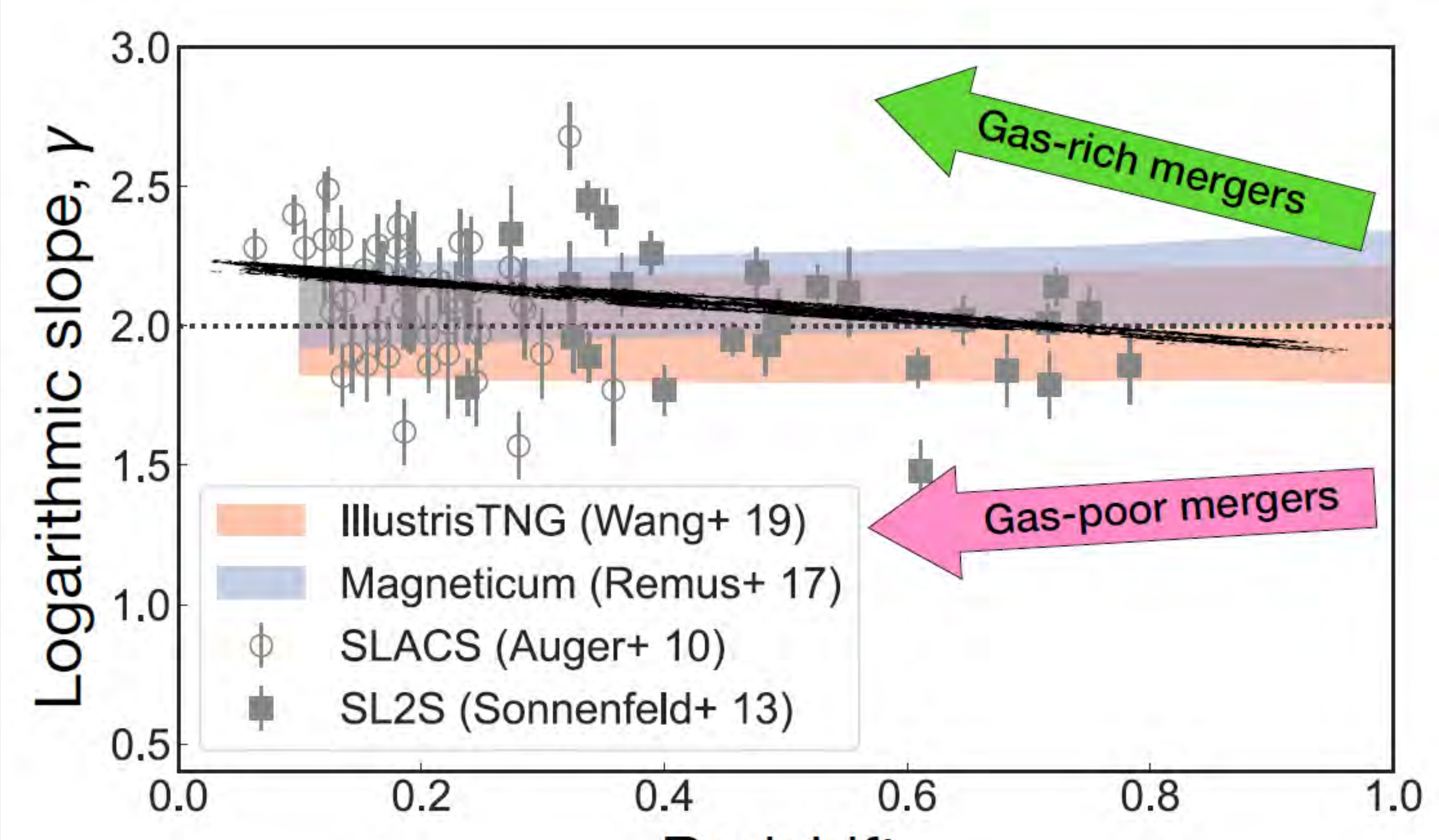

Shajib et al. 2021

PART3

Data and Methodology

Schematic of constraints

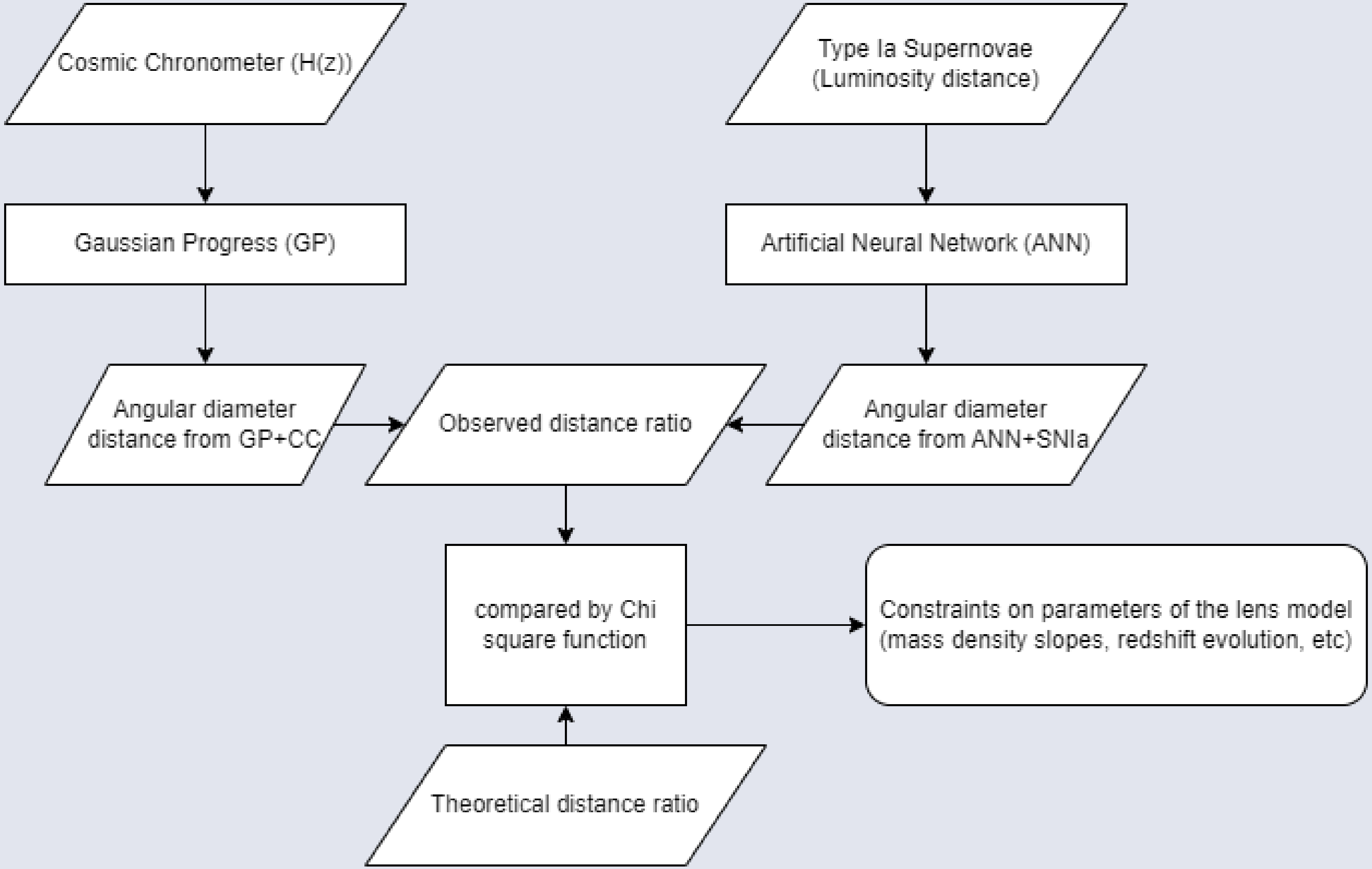

Schematic of constraints

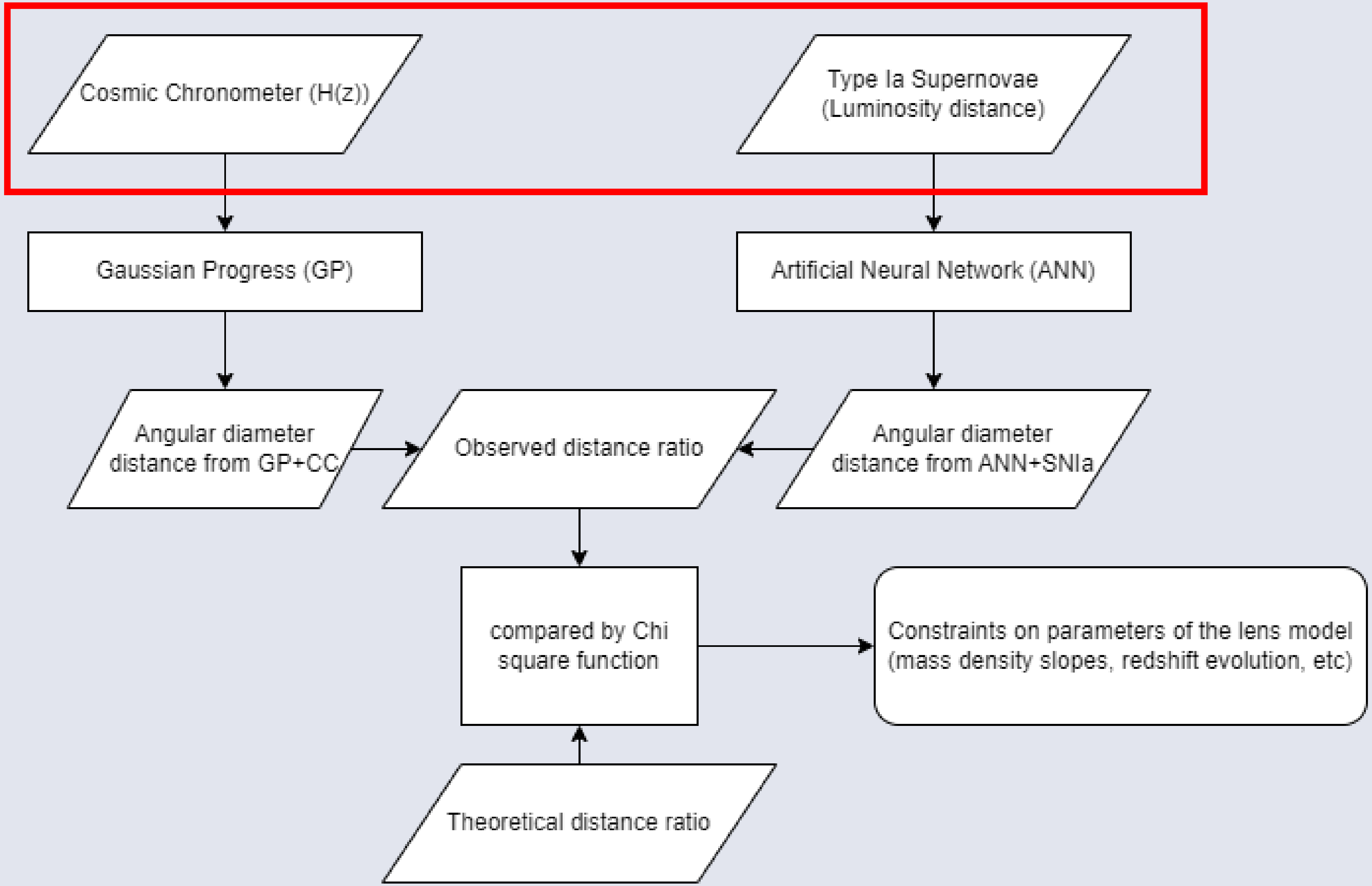

Model-independent observations

Schematic of constraints

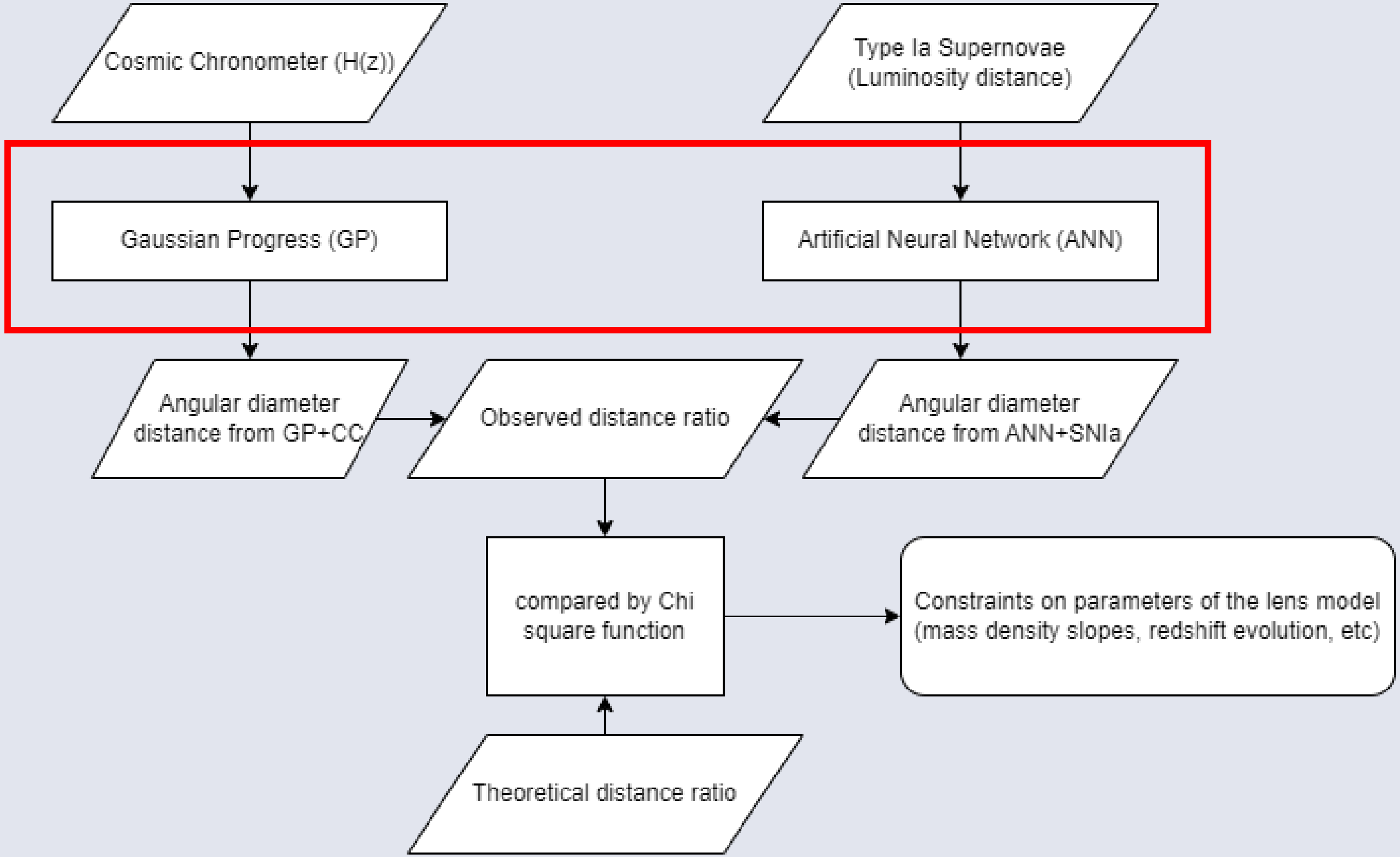

Non-parametric reconstruction methods

Schematic of constraints

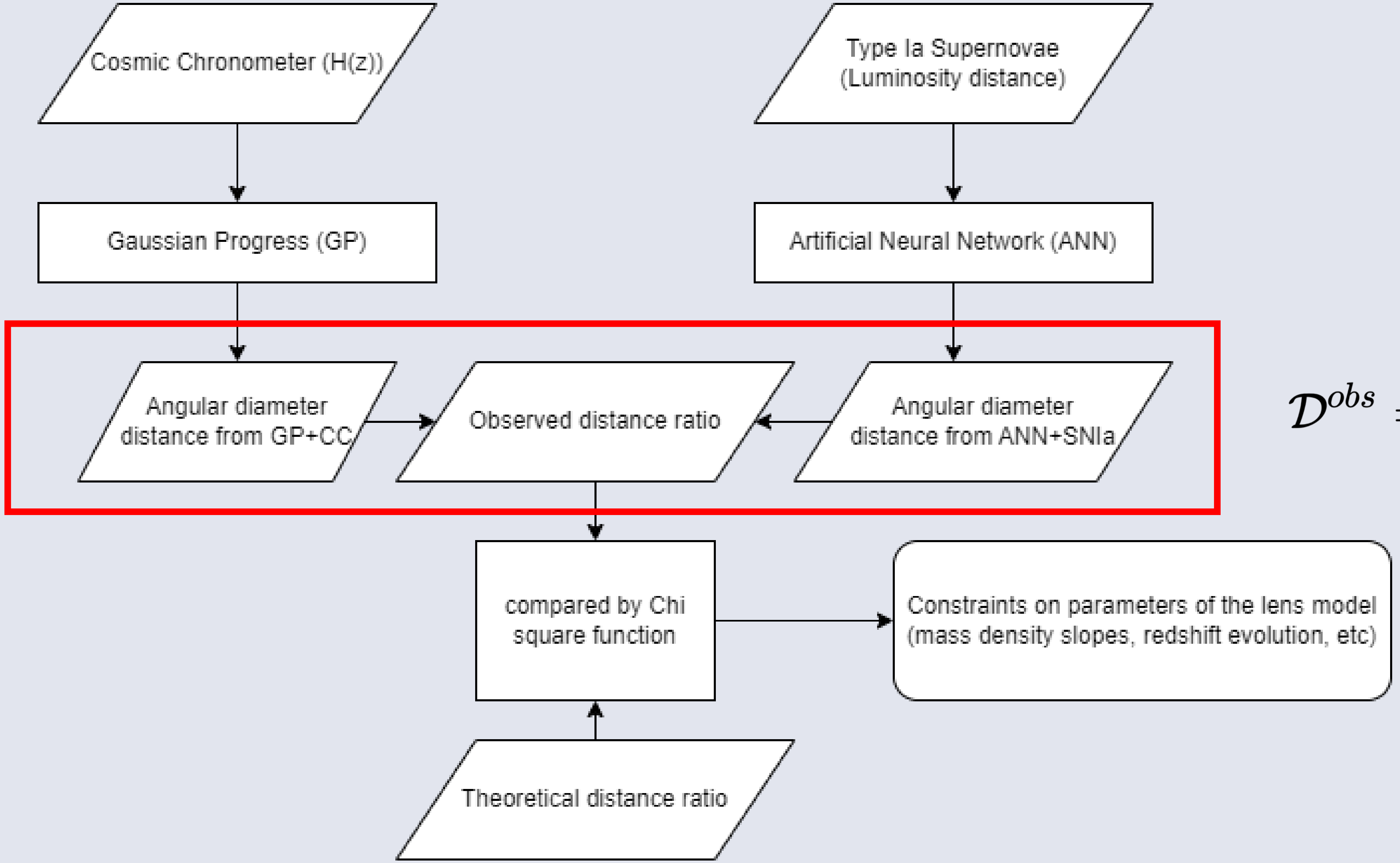

$$\mathcal{D}^{obs} = \frac{D_{ls}(z)}{D_s(z)}$$

Schematic of constraints

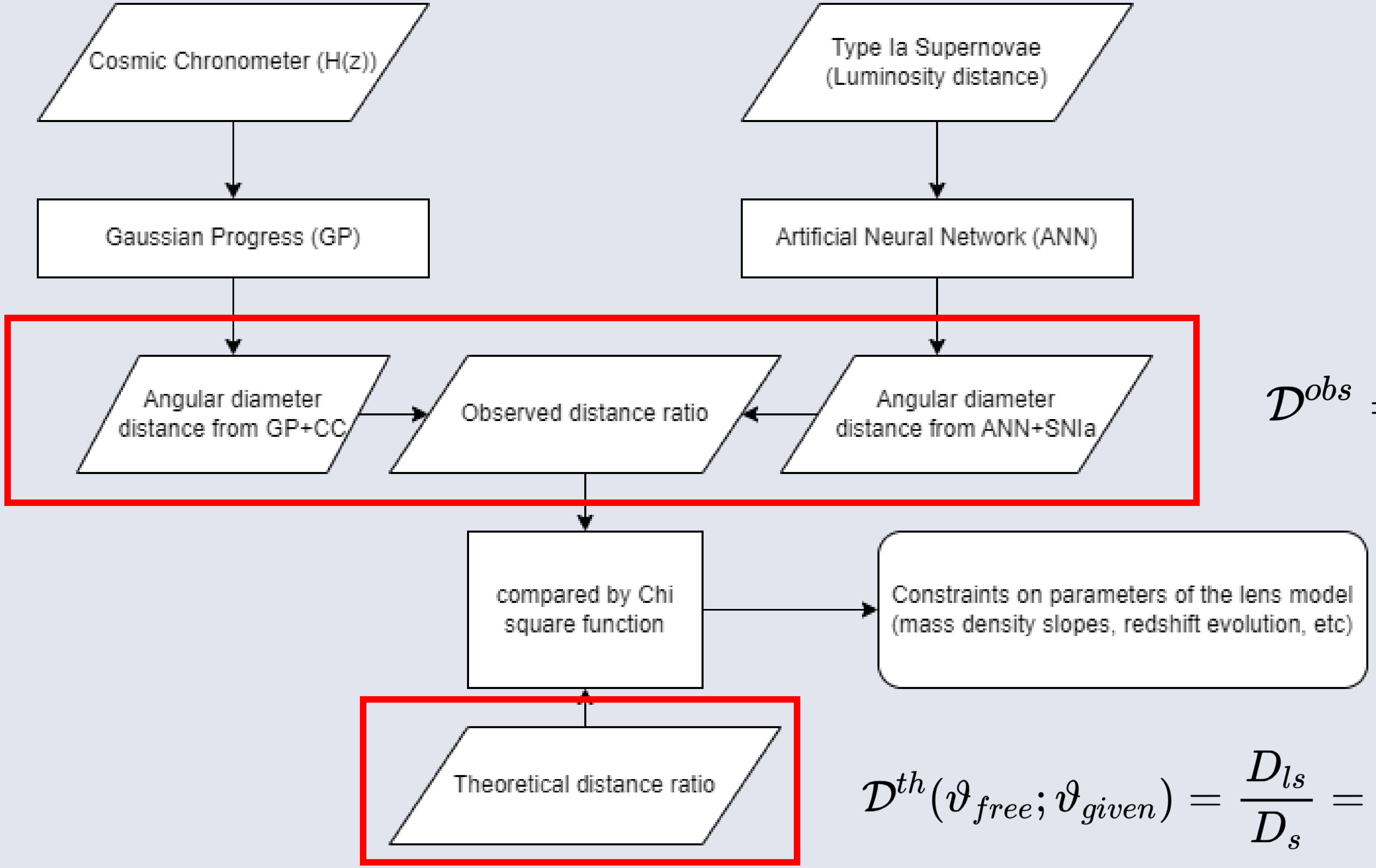

$$\mathcal{D}^{obs} = \frac{D_{ls}(z)}{D_s(z)}$$

$$\mathcal{D}^{th}(\vartheta_{free}; \vartheta_{given}) = \frac{D_{ls}}{D_s} = \frac{c^2}{4\pi}\frac{\theta_E}{\sigma_{ap}^2}\left(\frac{\theta_E}{\theta_{ap}}\right)^{\gamma-2} f^{-1}(\gamma, \delta, \beta)$$

SGL data

1. **LSD**
   5 systems from the Lenses Structure & Dynamics (LSD) Survey
2. **SL2S**
   26 systems from the Strong Lensing Legacy Survey (SL2S).
3. **SLACS**
   57 systems from the Sloan Lens ACS Survey (SLACS).
4. **S4TM**
   38 systems from the SLACS for the Masses (S4TM).
5. **BELLS**
   21 systems from the BOSS Emission-Line Lens Survey (BELLS).
6. **BELLS GALLERY**
   14 systems from the BELLS for GALaxy-Ly EmitteR sYstems.

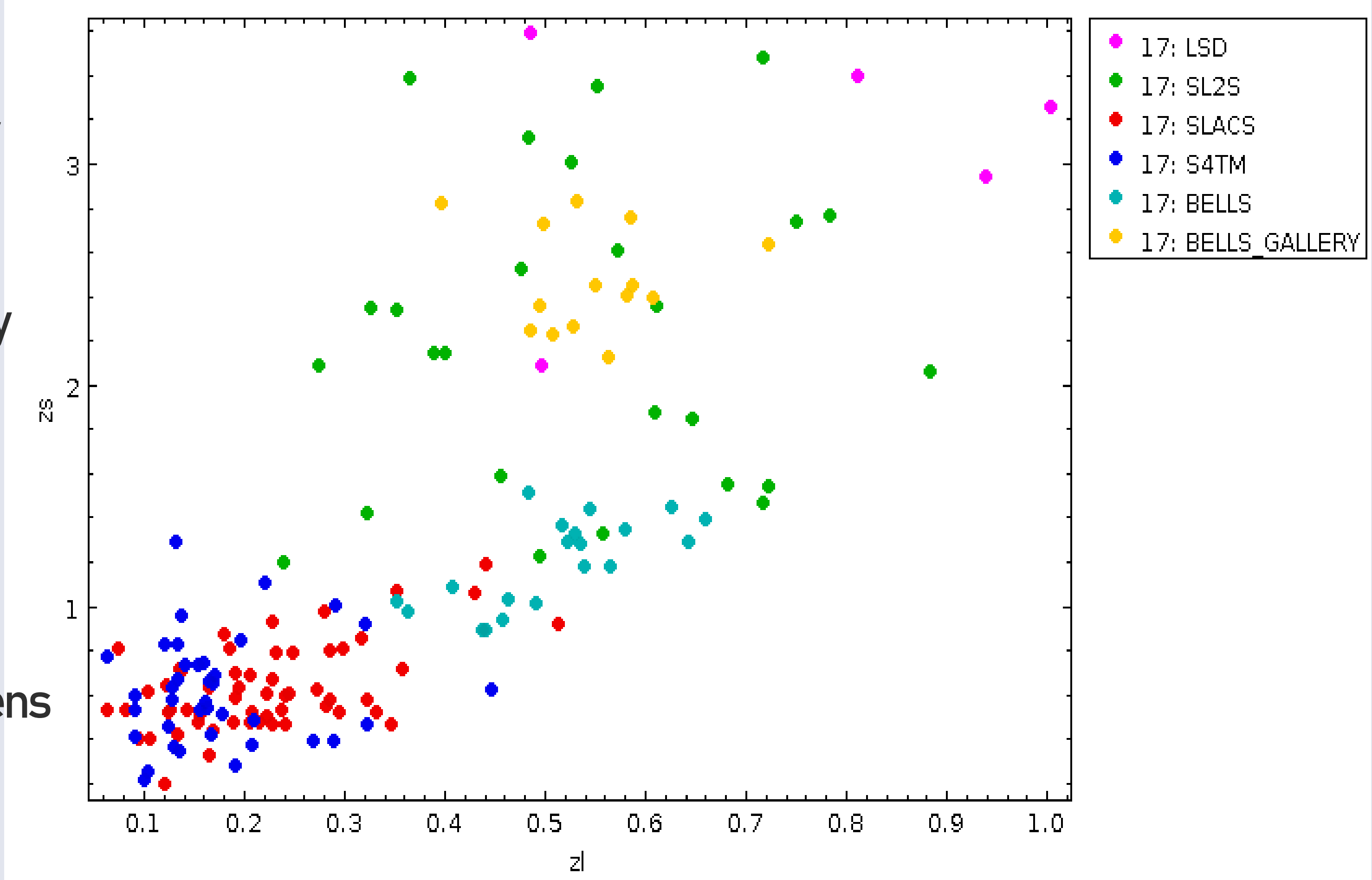

Luminosity distance

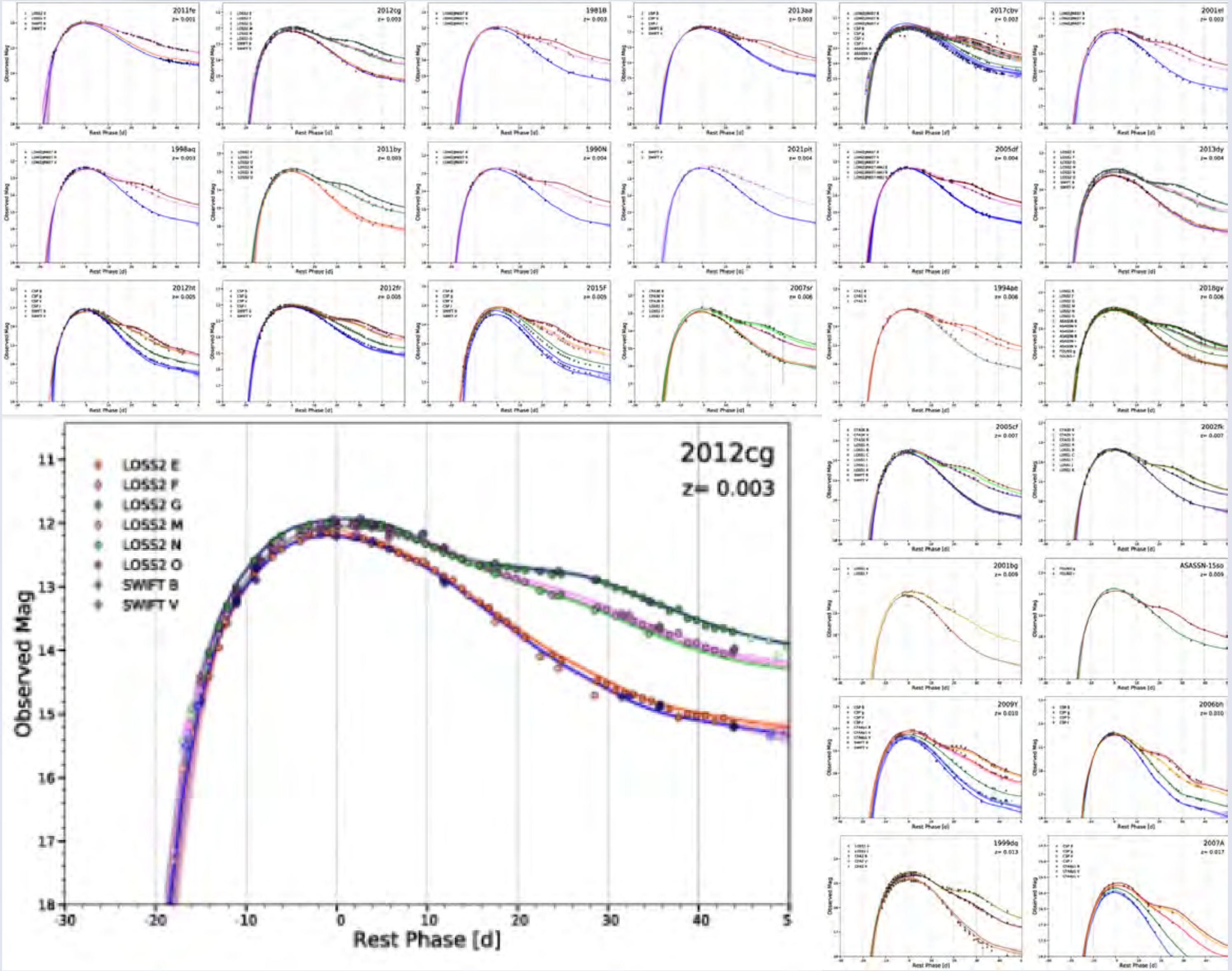

Pantheon+

1550 spectroscopically confirmed Type Ia supernovae.

Scolnic et al. 2022

$$D_A = \frac{1}{1+z} D_c$$

$$D_L = (1+z) D_c$$

H(z) data

Tomasetti et al. 2023

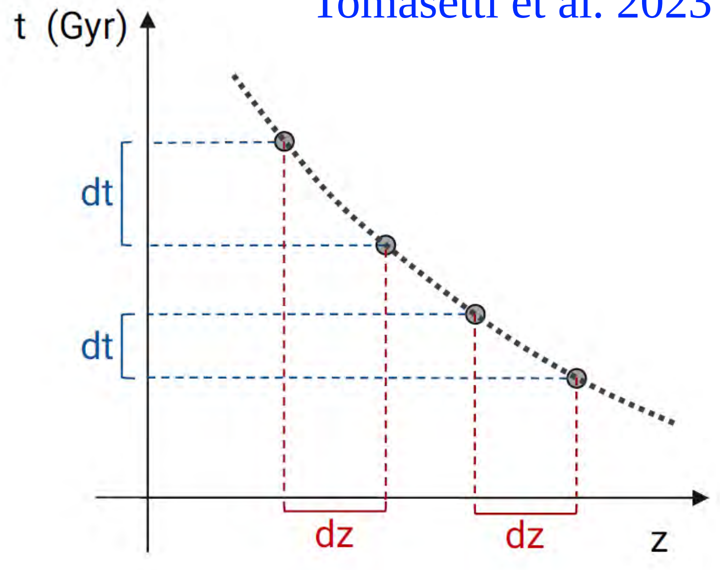

spectroscopic redshift

$$H(z) = \frac{\dot{a}}{a} = -\frac{1}{1+z}\frac{dz}{dt}$$

Jimenez & Loeb (2002)

can be traced with "chronometers"

Cosmic Chronometers: Passively evolving galaxies

They have rapidly accumulated mass typically within a brief period of less than 0.3 Gyr, predominantly at high redshifts (z>2~3)

$$D_A(z) = \frac{1}{1+z} D_C(z) = \frac{1}{1+z}\int_0^z \frac{c\,dz'}{H(z')}$$

Redshift	H(z)	Source	Ref.
0.0708	69.0 ± 19.68	CC	Zhang et al. (2014)
0.09	69.0 ± 12.0	CC	Jimenez et al. (2003)
0.12	68.6 ± 26.2	CC	Zhang et al. (2014)
0.17	83.0 ± 8.0	CC	Simon et al. (2005)
0.1791	78.0 ± 6.2	CC	Moresco et al. (2012)
0.1993	78.0 ± 6.9	CC	Moresco et al. (2012)
0.2	72.9 ± 29.6	CC	Zhang et al. (2014)
0.27	77.0 ± 14.0	CC	Simon et al. (2005)
0.28	88.8 ± 36.6	CC	Zhang et al. (2014)
0.3519	85.5 ± 15.7	CC	Moresco et al. (2012)
0.3802	86.2 ± 14.6	CC	Moresco et al. (2016)
0.4	95.0 ± 17.0	CC	Simon et al. (2005)
0.4004	79.9 ± 11.4	CC	Moresco et al. (2016)
0.4247	90.4 ± 12.8	CC	Moresco et al. (2016)
0.4497	96.3 ± 14.4	CC	Moresco et al. (2016)
0.47	89.0 ± 49.6	CC	Ratsimbazafy et al. (2017)
0.4783	83.8 ± 10.2	CC	Moresco et al. (2016)
0.48	97.0 ± 62.0	CC	Stern et al. (2010)
0.5929	107.0 ± 15.5	CC	Moresco et al. (2012)
0.6797	95.0 ± 10.5	CC	Moresco et al. (2012)
0.75	98.8 ± 33.6	CC	Borghi et al. (2022a)
0.7812	96.5 ± 12.5	CC	Moresco et al. (2012)
0.8	113.1 ± 15.1	CC	Jiao et al. (2023)
0.8754	124.5 ± 17.4	CC	Moresco et al. (2012)
0.88	90.0 ± 40.0	CC	Stern et al. (2010)
0.9	117.0 ± 23.0	CC	Simon et al. (2005)
1.037	133.5 ± 17.6	CC	Moresco et al. (2012)
1.26	135.0 ± 65.0	CC	Tomasetti et al. (2023)
1.3	168.0 ± 17.0	CC	Simon et al. (2005)
1.363	160.0 ± 33.8	CC	Moresco (2015)
1.43	177.0 ± 18.0	CC	Simon et al. (2005)
1.53	140.0 ± 14.0	CC	Simon et al. (2005)
1.75	202.0 ± 40.0	CC	Simon et al. (2005)
1.965	186.5 ± 50.6	CC	Moresco (2015)
2.34	227.0 ± 8.0	BAO	de Sainte Agathe et al. (2019)

Distance reconstruction

Gaussian Process (GP):

Assuming the given data and the points needed to be reconstructed following a joint Gaussian distribution

$$\begin{bmatrix} \mathbf{y} \\ \mathbf{f} \end{bmatrix} \sim \mathcal{N}\left(\begin{bmatrix} \mu(\mathbf{Z}) \\ \mu(\mathbf{Z}_1) \end{bmatrix}, \begin{bmatrix} K(Z,Z) & K(Z,Z_1) \\ K(Z_1,Z) & K(Z_1,Z_1) \end{bmatrix} \right)$$

Artificial Neural Network (ANN):

Non-linear mathematical function

Structured in layers and all the neurons from each layer are interconnected by weighted connections.

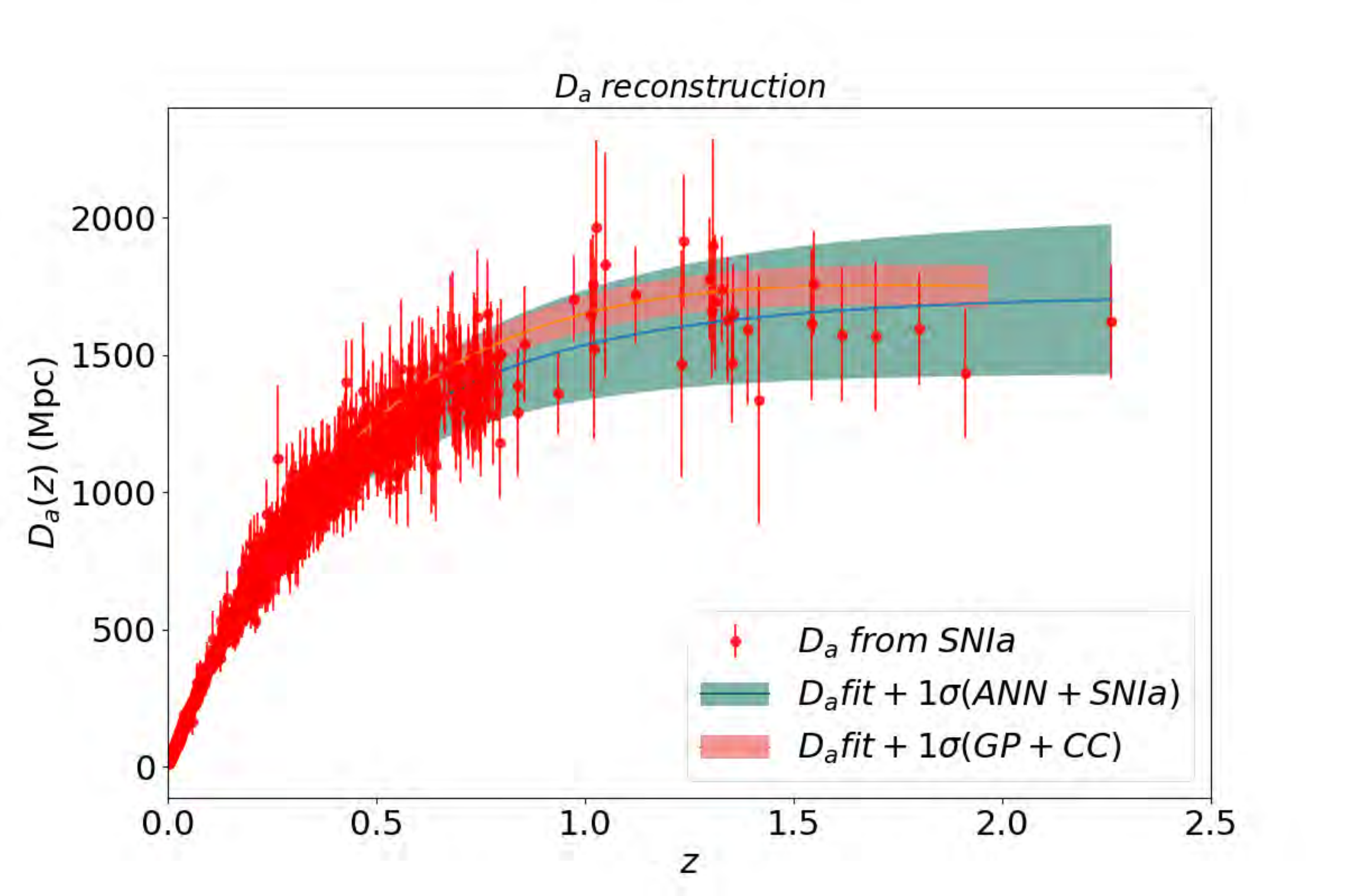

H(z) data

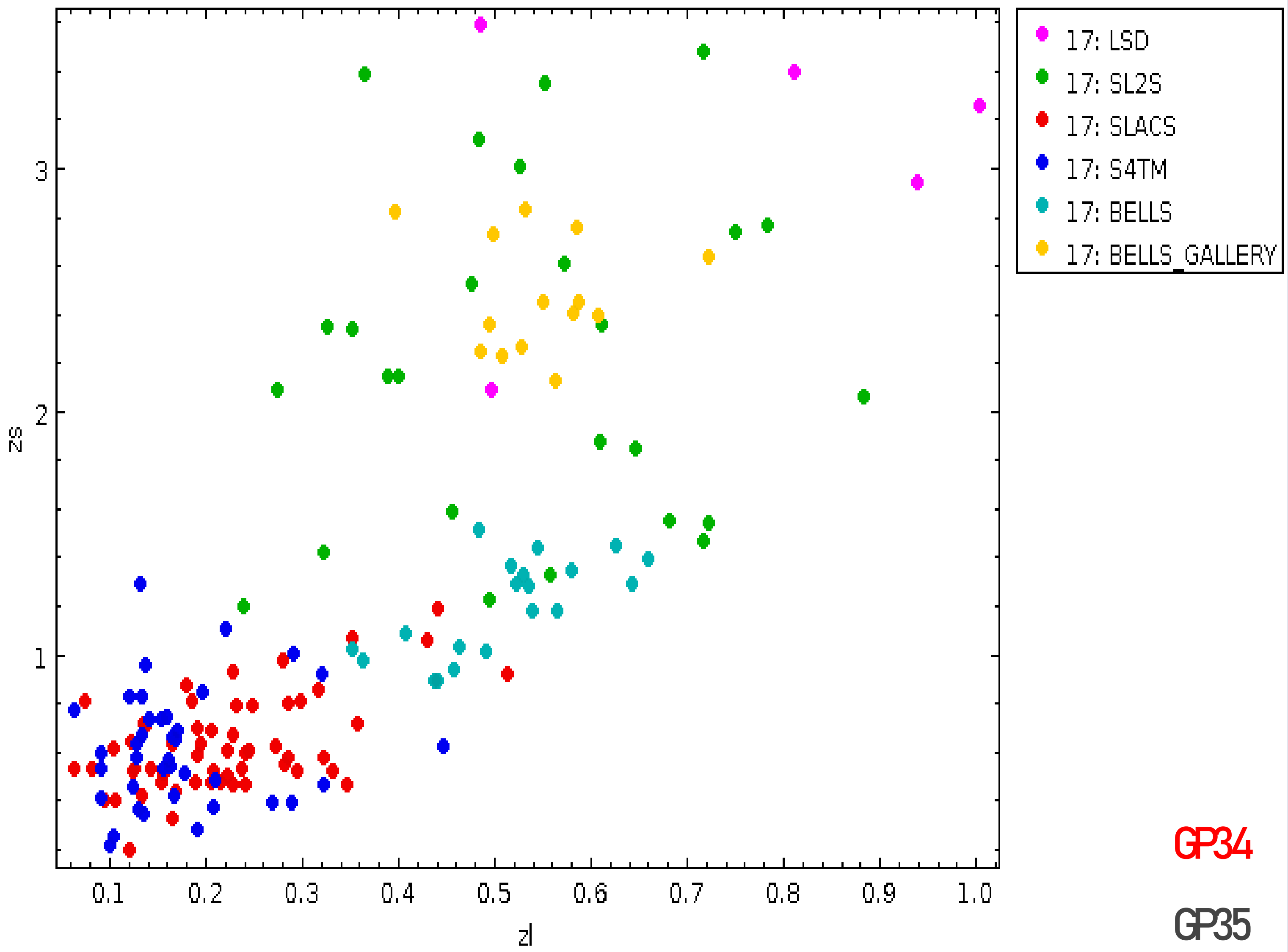

GP34

GP35

Redshift	H(z)	Source	Ref.
0.0708	69.0 ± 19.68	CC	Zhang et al. (2014)
0.09	69.0 ± 12.0	CC	Jimenez et al. (2003)
0.12	68.6 ± 26.2	CC	Zhang et al. (2014)
0.17	83.0 ± 8.0	CC	Simon et al. (2005)
0.1791	78.0 ± 6.2	CC	Moresco et al. (2012)
0.1993	78.0 ± 6.9	CC	Moresco et al. (2012)
0.2	72.9 ± 29.6	CC	Zhang et al. (2014)
0.27	77.0 ± 14.0	CC	Simon et al. (2005)
0.28	88.8 ± 36.6	CC	Zhang et al. (2014)
0.3519	85.5 ± 15.7	CC	Moresco et al. (2012)
0.3802	86.2 ± 14.6	CC	Moresco et al. (2016)
0.4	95.0 ± 17.0	CC	Simon et al. (2005)
0.4004	79.9 ± 11.4	CC	Moresco et al. (2016)
0.4247	90.4 ± 12.8	CC	Moresco et al. (2016)
0.4497	96.3 ± 14.4	CC	Moresco et al. (2016)
0.47	89.0 ± 49.6	CC	Ratsimbazafy et al. (2017)
0.4783	83.8 ± 10.2	CC	Moresco et al. (2016)
0.48	97.0 ± 62.0	CC	Stern et al. (2010)
0.5929	107.0 ± 15.5	CC	Moresco et al. (2012)
0.6797	95.0 ± 10.5	CC	Moresco et al. (2012)
0.75	98.8 ± 33.6	CC	Borghi et al. (2022a)
0.7812	96.5 ± 12.5	CC	Moresco et al. (2012)
0.8	113.1 ± 15.1	CC	Jiao et al. (2023)
0.8754	124.5 ± 17.4	CC	Moresco et al. (2012)
0.88	90.0 ± 40.0	CC	Stern et al. (2010)
0.9	117.0 ± 23.0	CC	Simon et al. (2005)
1.037	133.5 ± 17.6	CC	Moresco et al. (2012)
1.26	135.0 ± 65.0	CC	Tomasetti et al. (2023)
1.3	168.0 ± 17.0	CC	Simon et al. (2005)
1.363	160.0 ± 33.8	CC	Moresco (2015)
1.43	177.0 ± 18.0	CC	Simon et al. (2005)
1.53	140.0 ± 14.0	CC	Simon et al. (2005)
1.75	202.0 ± 40.0	CC	Simon et al. (2005)
1.965	186.5 ± 50.6	CC	Moresco (2015)
2.34	227.0 ± 8.0	BAO	de Sainte Agathe et al. (2019)

H(z) data

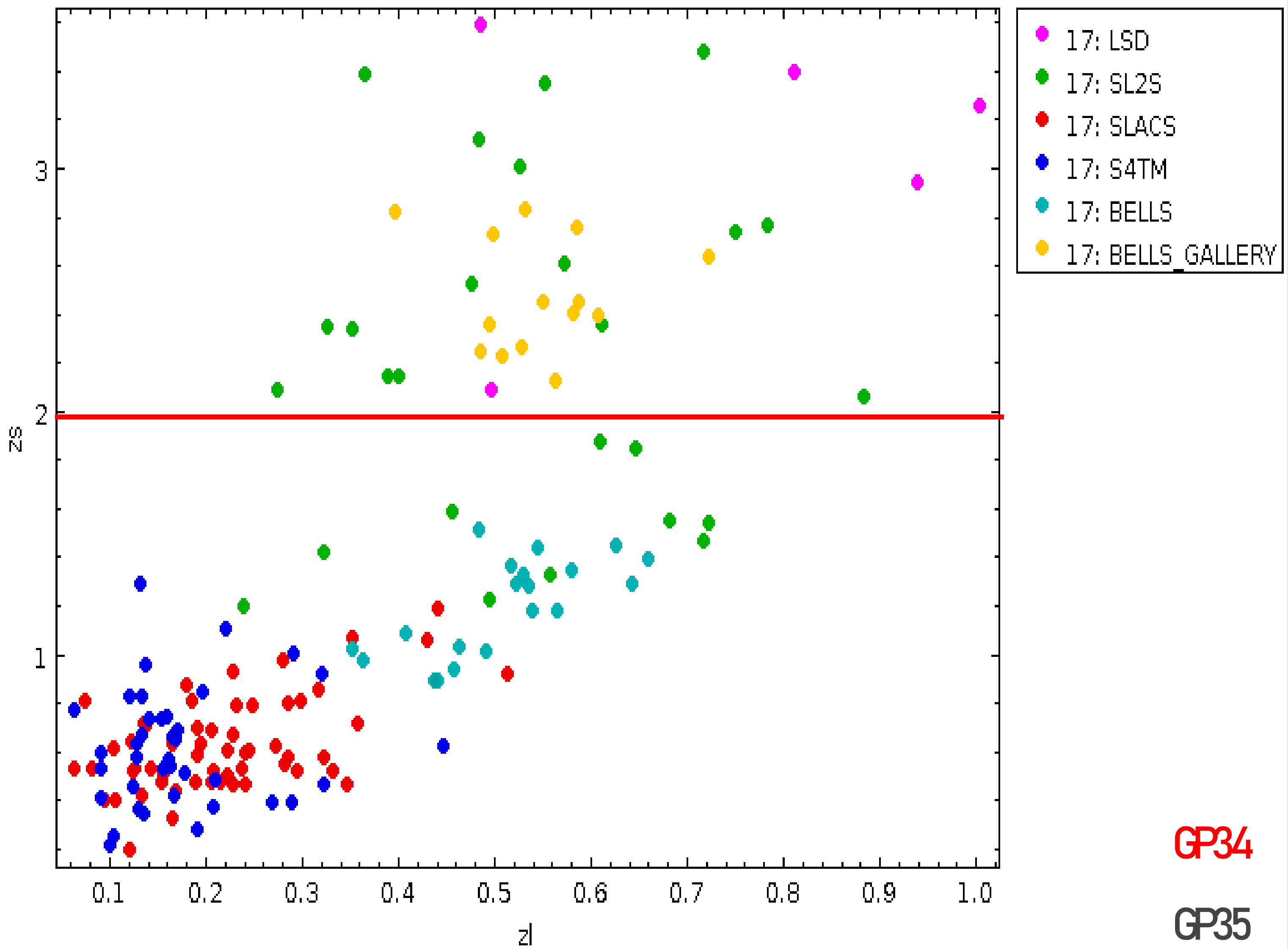

GP34

GP35

Redshift	H(z)	Source	Ref.
0.0708	69.0 ± 19.68	CC	Zhang et al. (2014)
0.09	69.0 ± 12.0	CC	Jimenez et al. (2003)
0.12	68.6 ± 26.2	CC	Zhang et al. (2014)
0.17	83.0 ± 8.0	CC	Simon et al. (2005)
0.1791	78.0 ± 6.2	CC	Moresco et al. (2012)
0.1993	78.0 ± 6.9	CC	Moresco et al. (2012)
0.2	72.9 ± 29.6	CC	Zhang et al. (2014)
0.27	77.0 ± 14.0	CC	Simon et al. (2005)
0.28	88.8 ± 36.6	CC	Zhang et al. (2014)
0.3519	85.5 ± 15.7	CC	Moresco et al. (2012)
0.3802	86.2 ± 14.6	CC	Moresco et al. (2016)
0.4	95.0 ± 17.0	CC	Simon et al. (2005)
0.4004	79.9 ± 11.4	CC	Moresco et al. (2016)
0.4247	90.4 ± 12.8	CC	Moresco et al. (2016)
0.4497	96.3 ± 14.4	CC	Moresco et al. (2016)
0.47	89.0 ± 49.6	CC	Ratsimbazafy et al. (2017)
0.4783	83.8 ± 10.2	CC	Moresco et al. (2016)
0.48	97.0 ± 62.0	CC	Stern et al. (2010)
0.5929	107.0 ± 15.5	CC	Moresco et al. (2012)
0.6797	95.0 ± 10.5	CC	Moresco et al. (2012)
0.75	98.8 ± 33.6	CC	Borghi et al. (2022a)
0.7812	96.5 ± 12.5	CC	Moresco et al. (2012)
0.8	113.1 ± 15.1	CC	Jiao et al. (2023)
0.8754	124.5 ± 17.4	CC	Moresco et al. (2012)
0.88	90.0 ± 40.0	CC	Stern et al. (2010)
0.9	117.0 ± 23.0	CC	Simon et al. (2005)
1.037	133.5 ± 17.6	CC	Moresco et al. (2012)
1.26	135.0 ± 65.0	CC	Tomasetti et al. (2023)
1.3	168.0 ± 17.0	CC	Simon et al. (2005)
1.363	160.0 ± 33.8	CC	Moresco (2015)
1.43	177.0 ± 18.0	CC	Simon et al. (2005)
1.53	140.0 ± 14.0	CC	Simon et al. (2005)
1.75	202.0 ± 40.0	CC	Simon et al. (2005)
1.965	186.5 ± 50.6	CC	Moresco (2015)
2.34	227.0 ± 8.0	BAO	de Sainte Agathe et al. (2019)

H(z) data

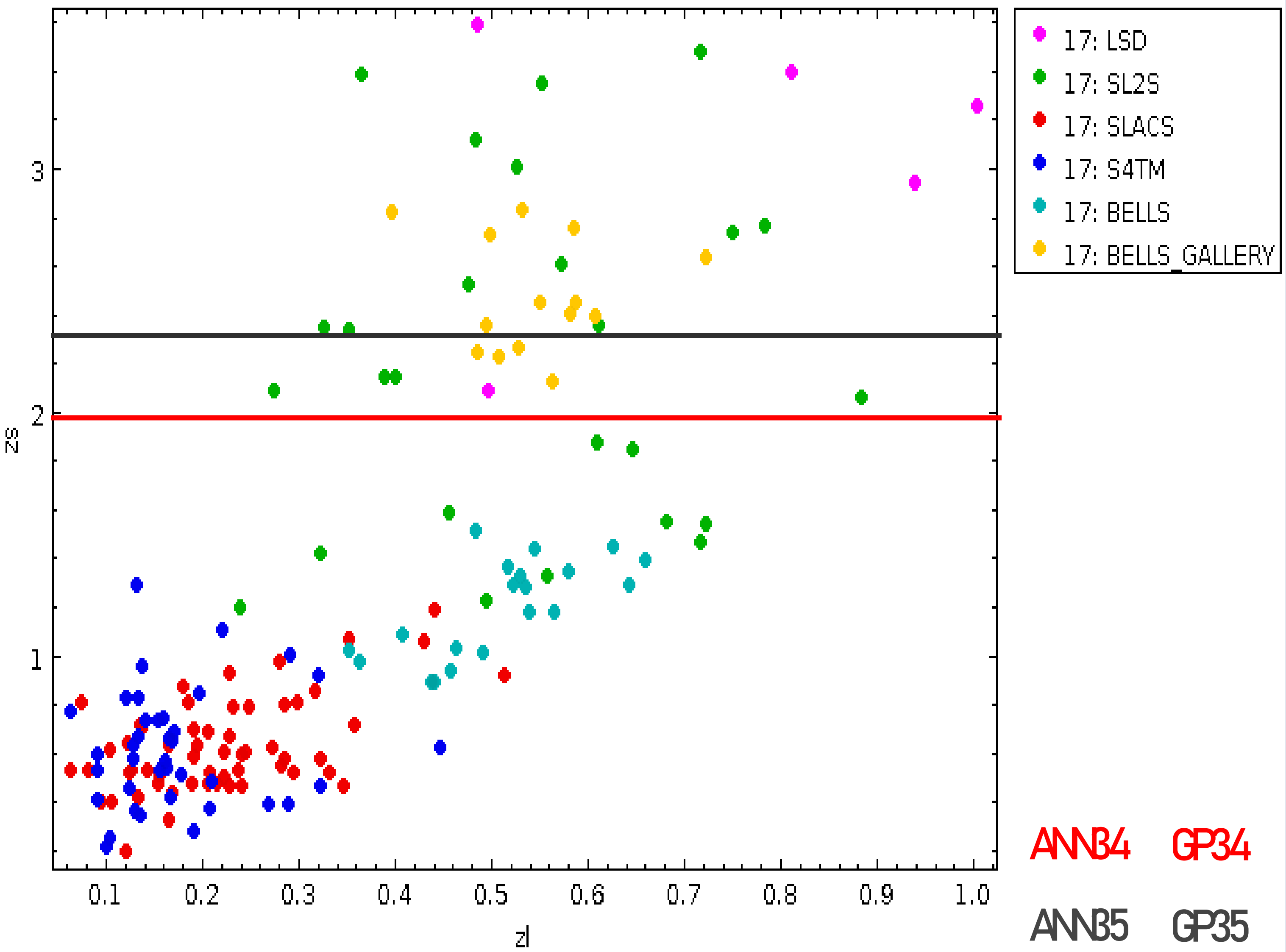

ANN34 GP34

ANN35 GP35

Redshift	H(z)	Source	Ref.
0.0708	69.0 ± 19.68	CC	Zhang et al. (2014)
0.09	69.0 ± 12.0	CC	Jimenez et al. (2003)
0.12	68.6 ± 26.2	CC	Zhang et al. (2014)
0.17	83.0 ± 8.0	CC	Simon et al. (2005)
0.1791	78.0 ± 6.2	CC	Moresco et al. (2012)
0.1993	78.0 ± 6.9	CC	Moresco et al. (2012)
0.2	72.9 ± 29.6	CC	Zhang et al. (2014)
0.27	77.0 ± 14.0	CC	Simon et al. (2005)
0.28	88.8 ± 36.6	CC	Zhang et al. (2014)
0.3519	85.5 ± 15.7	CC	Moresco et al. (2012)
0.3802	86.2 ± 14.6	CC	Moresco et al. (2016)
0.4	95.0 ± 17.0	CC	Simon et al. (2005)
0.4004	79.9 ± 11.4	CC	Moresco et al. (2016)
0.4247	90.4 ± 12.8	CC	Moresco et al. (2016)
0.4497	96.3 ± 14.4	CC	Moresco et al. (2016)
0.47	89.0 ± 49.6	CC	Ratsimbazafy et al. (2017)
0.4783	83.8 ± 10.2	CC	Moresco et al. (2016)
0.48	97.0 ± 62.0	CC	Stern et al. (2010)
0.5929	107.0 ± 15.5	CC	Moresco et al. (2012)
0.6797	95.0 ± 10.5	CC	Moresco et al. (2012)
0.75	98.8 ± 33.6	CC	Borghi et al. (2022a)
0.7812	96.5 ± 12.5	CC	Moresco et al. (2012)
0.8	113.1 ± 15.1	CC	Jiao et al. (2023)
0.8754	124.5 ± 17.4	CC	Moresco et al. (2012)
0.88	90.0 ± 40.0	CC	Stern et al. (2010)
0.9	117.0 ± 23.0	CC	Simon et al. (2005)
1.037	133.5 ± 17.6	CC	Moresco et al. (2012)
1.26	135.0 ± 65.0	CC	Tomasetti et al. (2023)
1.3	168.0 ± 17.0	CC	Simon et al. (2005)
1.363	160.0 ± 33.8	CC	Moresco (2015)
1.43	177.0 ± 18.0	CC	Simon et al. (2005)
1.53	140.0 ± 14.0	CC	Simon et al. (2005)
1.75	202.0 ± 40.0	CC	Simon et al. (2005)
1.965	186.5 ± 50.6	CC	Moresco (2015)
2.34	227.0 ± 8.0	BAO	de Sainte Agathe et al. (2019)

Anisotropy prior

Zhu et al. 2023

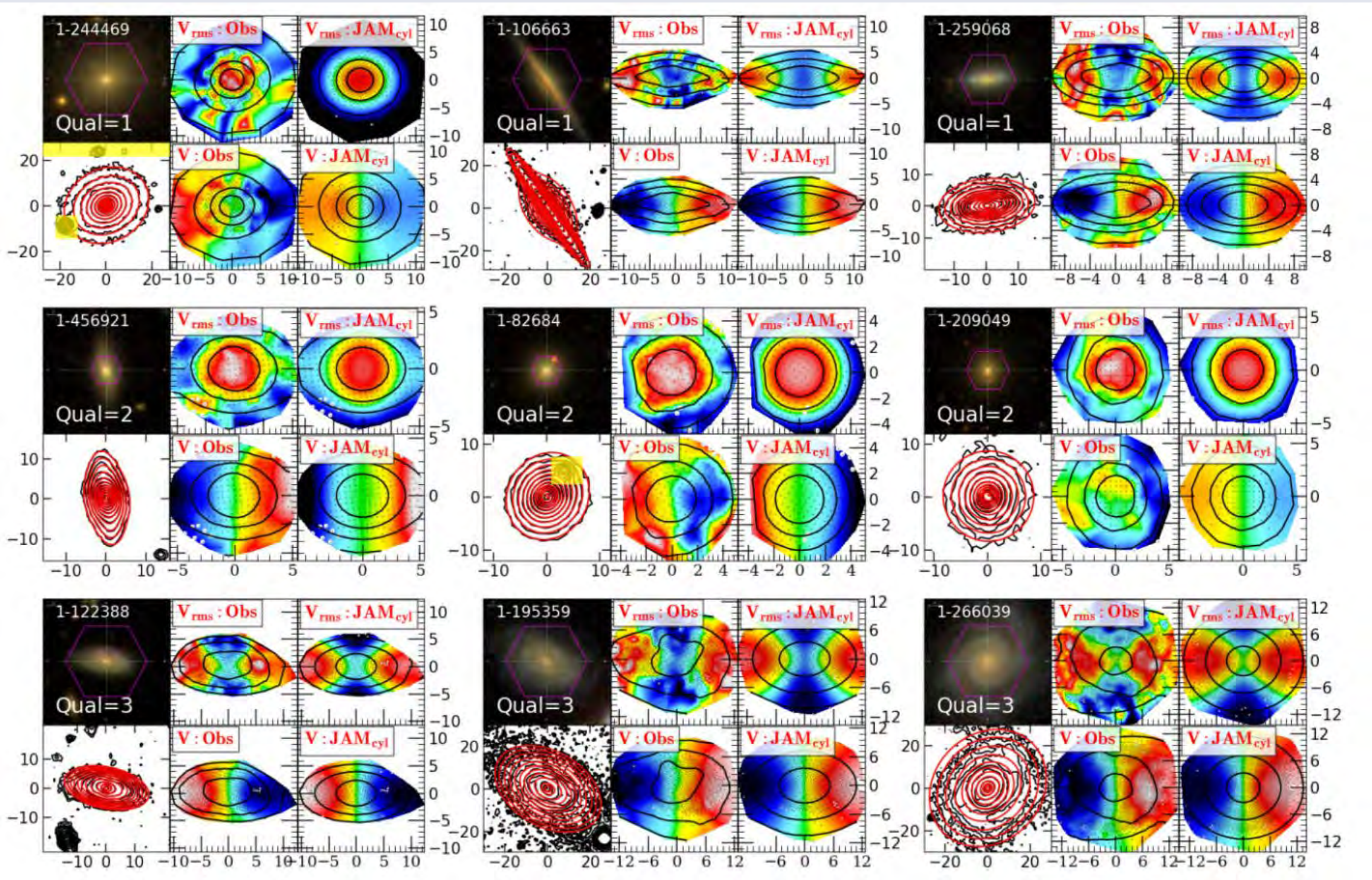

- Data from MaNGA survey (SDSS Data release 17)
- ~ 10,000 galaxies
- Observations based on integral field unit (IFU)
- Axisymmetric Jeans Anisotropic Modeling (JAM) method
- Different mass model: mass-follow-light, stellar mass + NFW, stellar mass + fixed NFW, stellar mass + general NFW

$$\rho_L(r) = \rho_L r^{-\delta}$$

$$\rho_{tot}(r) = \rho_{tot} r^{-\gamma}$$

$$\beta(r) = 1 - \frac{\langle \sigma_\theta^2 \rangle}{\langle \sigma_r^2 \rangle},$$

Anisotropy prior

Gerhard et al. 2001

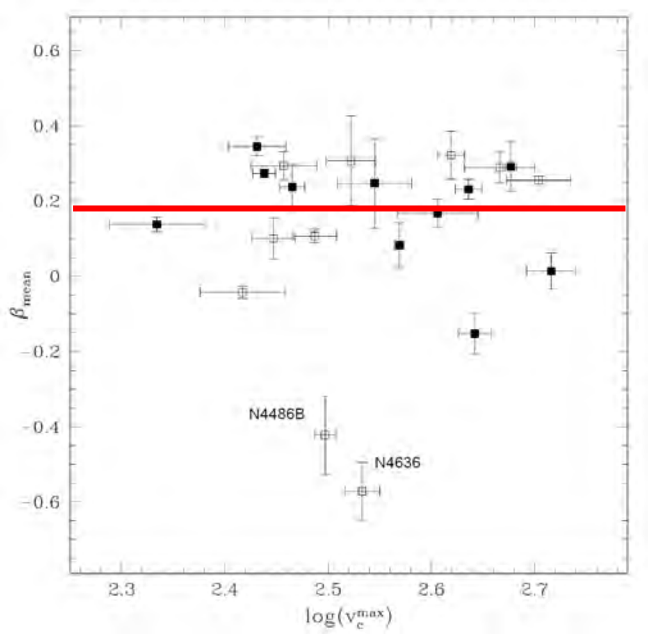

Gaussian Prior

N(0.18,0.13^2)

Bolton et al. 2006

Guerrini et al. 2024

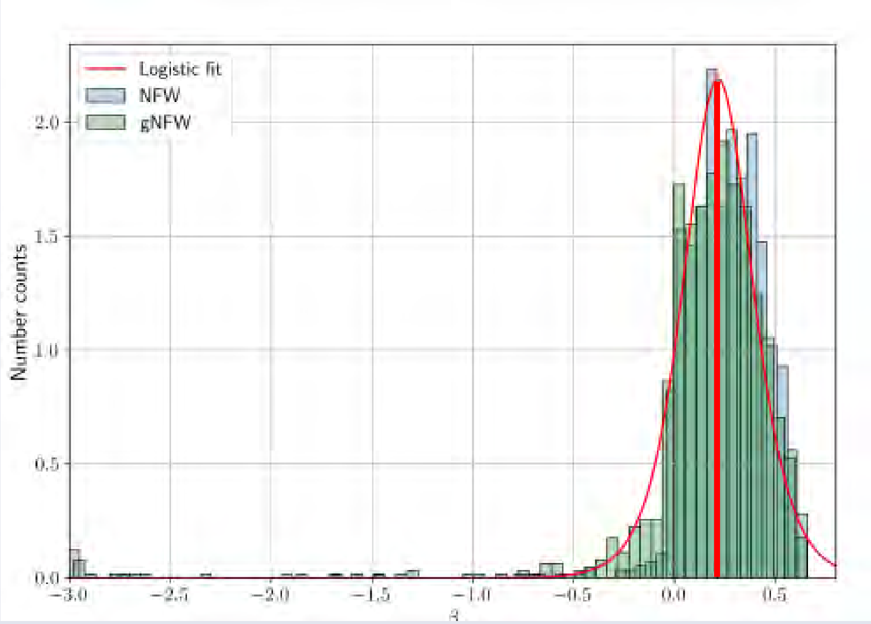

Gaussian Prior

N(0.22,0.2^2)

$$|\beta_{NFW} - \beta_{gNFW}| < 0.05.$$

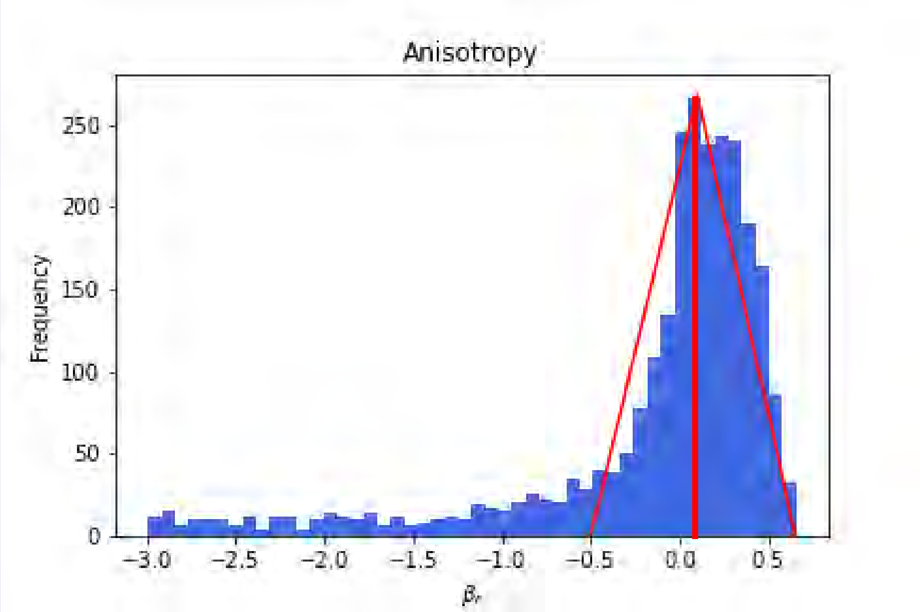

Triangular Prior

Tri(-0.5,0.656, mode=0.102)

Density slope constraints

1. **Single density slope model ($\gamma = \delta$)**

   Adopting a uniform logarithmic density distribution for both the total and luminous mass components.

   1. **Individual constraining**
   2. **Fixed-bin approach**

      Grouping lenses by the redshift of the lensing objects within fixed-size bins.
   3. **Direct constraining**

      Considering a linear relationship between the total mass logarithmic slope and redshift $\gamma_i = \gamma_0 + \gamma_s * z_l$, as a universal characteristic of the sample.

2. **General spherical power-law model ($\gamma \neq \delta$)**
   1. **Non-evolving**
   2. **Linear evolution or CPL-like evolution**

$$\gamma_i = \gamma_0 + \gamma_s * z_l$$
$$\delta_i = \delta_0 + \delta_s * z_l$$

$$\gamma_i = \gamma_0 + \gamma_s * \frac{z_l}{1+z_l}$$
$$\delta_i = \delta_0 + \delta_s * \frac{z_l}{1+z_l}$$

PART 4

Results

Individual constraining

Single slope

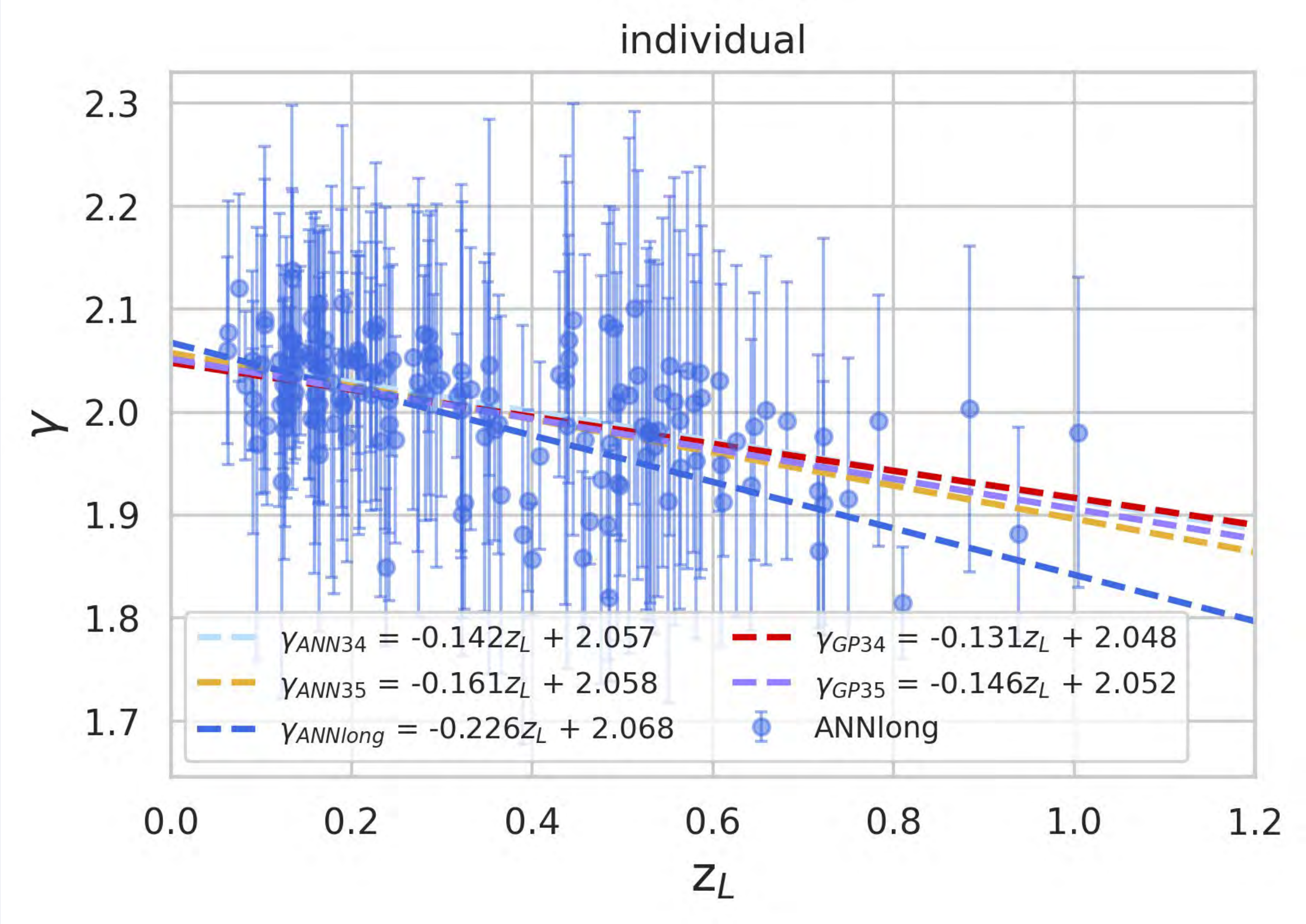

- Despite considerable uncertainties, results show that both reconstruction combinations suggest the same negative evolution trend for the logarithmic density slope of lensing galaxies as the redshift increasing.

Binning approach

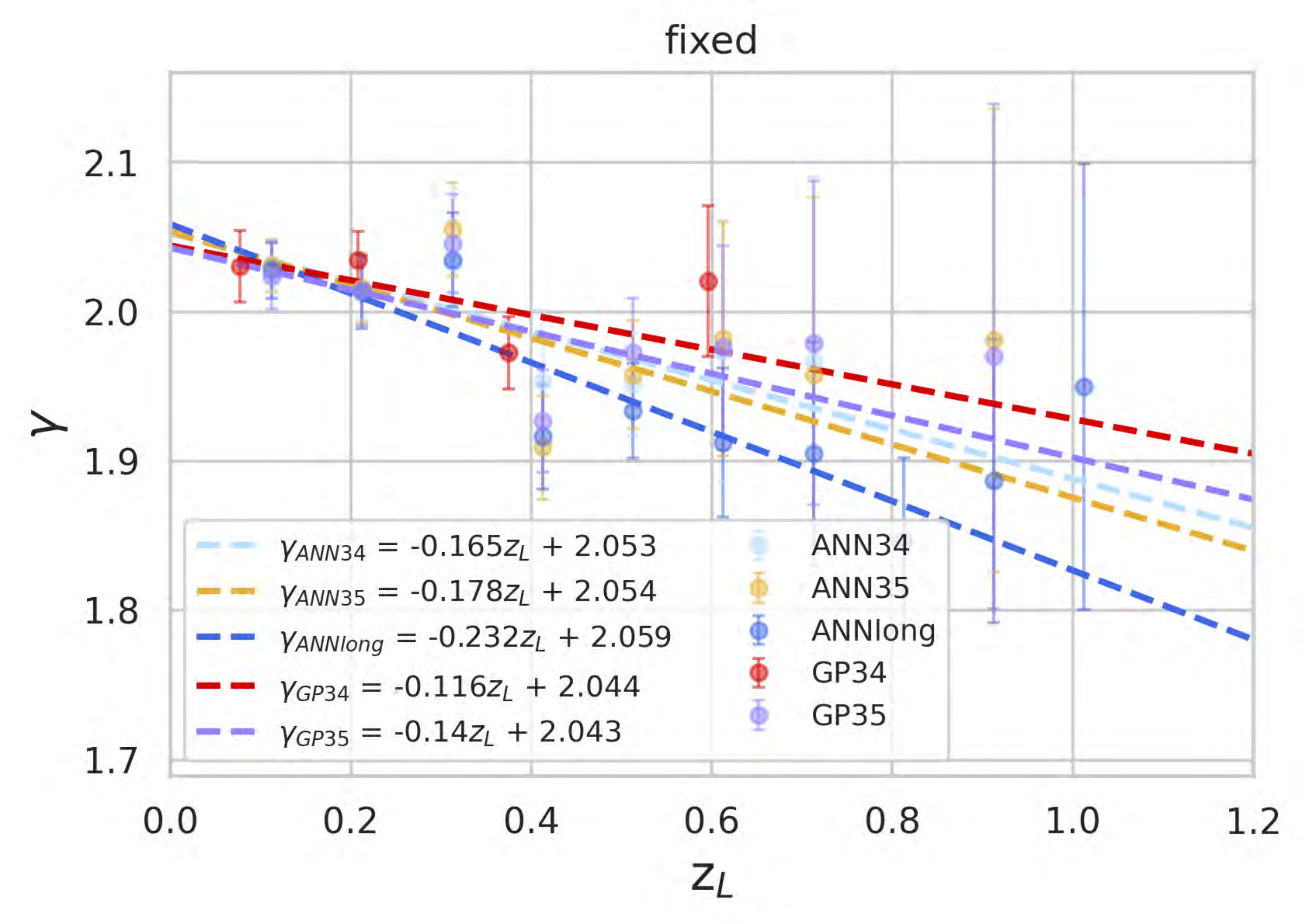

Single slope

- Due to uneven occupation of bins, i.e. much less at higher z, uncertainty increases in these bins.
- The variation in results among different reconstruction combinations is more pronounced at higher redshifts.
- In general, results from ANN+SNIa suggest a slight steeper redshift evolution than results from GP+CC.
- Compared to the individual constraining, the variation in the redshift evolution slope from ANN34 to ANN is less significant when using binning.

Direct method & summary

Single slope

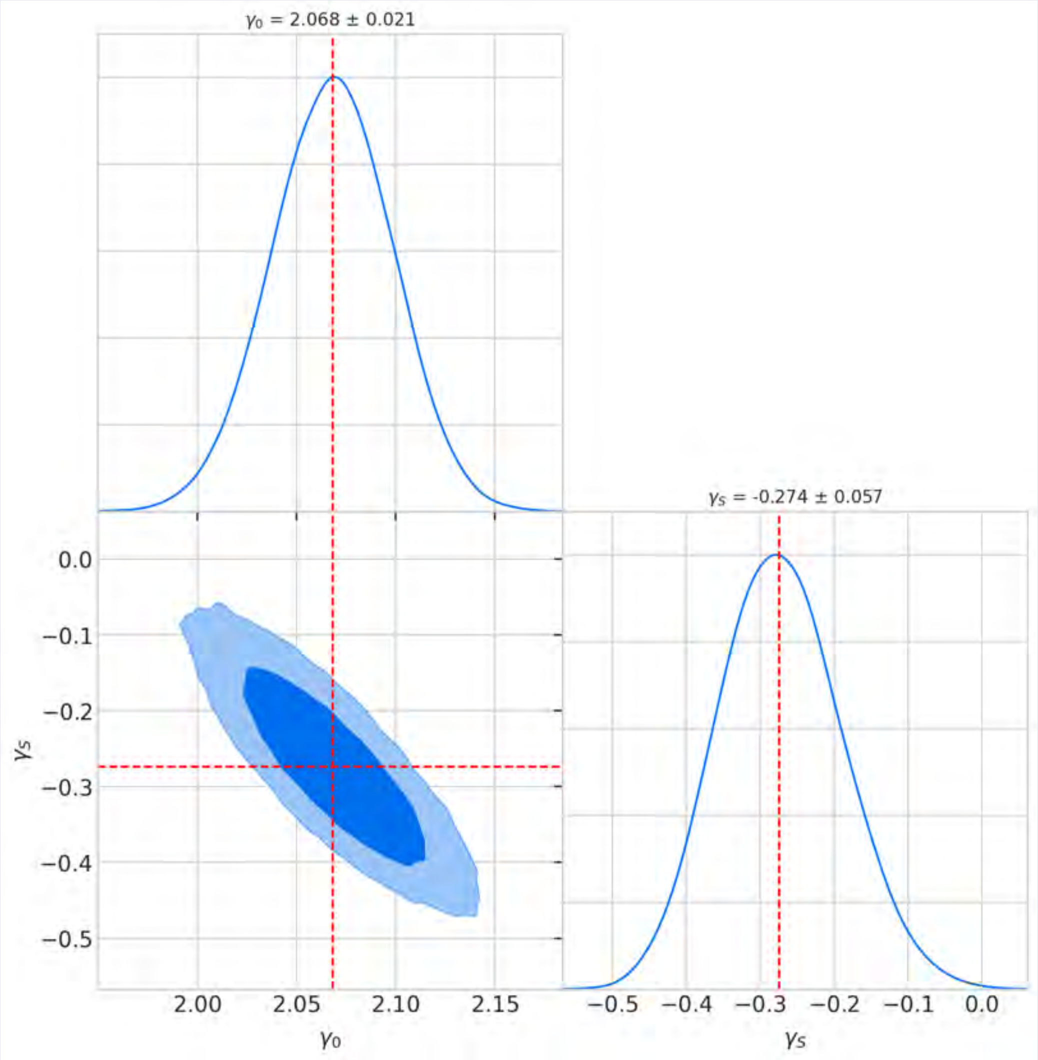

Direct method & summary

Single slope

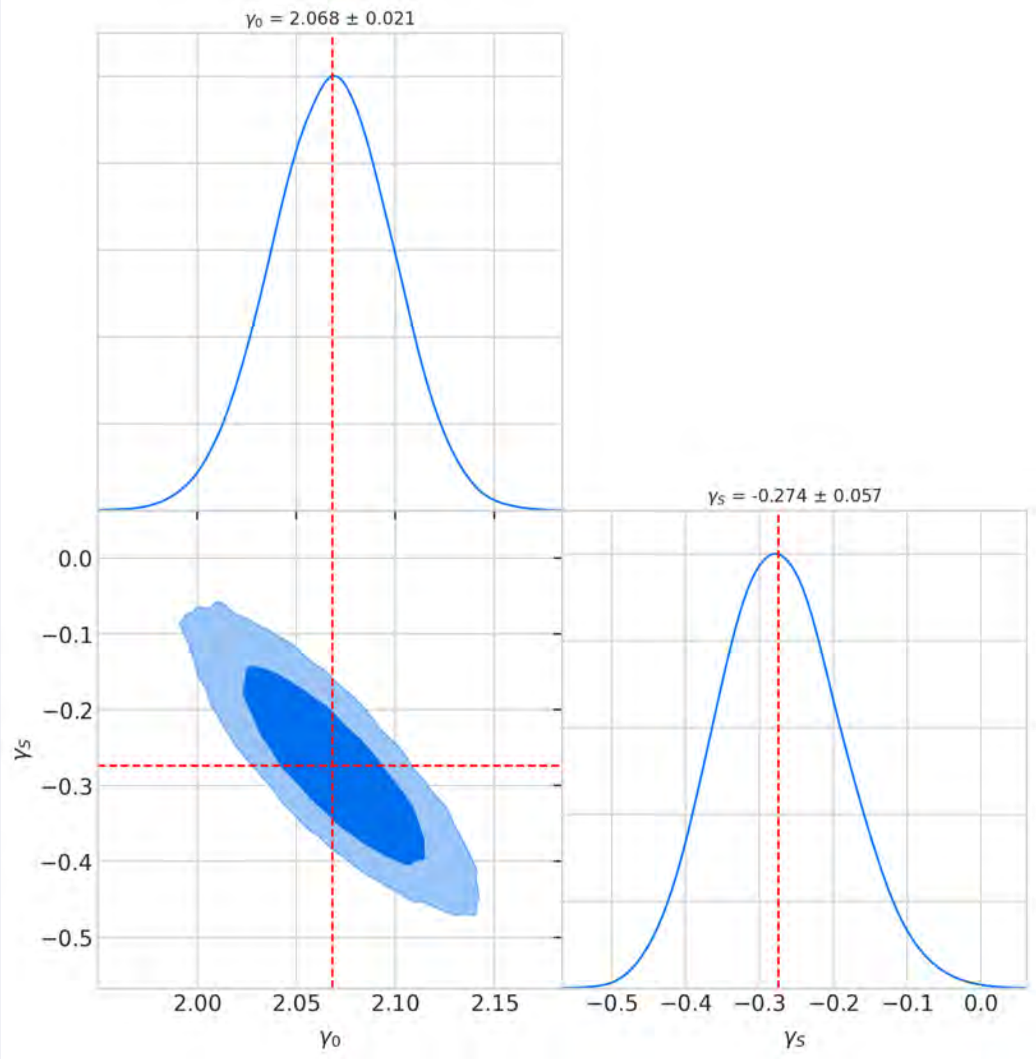

Approach	Parameters	GP34	ANN34	ANNlong
Individual	γ_0	2.048 ± 0.011	2.057 ± 0.011	2.068 ± 0.01
	$\frac{\partial\gamma}{\partial z_l}$	-0.131 ± 0.041	-0.142 ± 0.041	-0.226 ± 0.027
Fixed z bins	γ_0	2.044 ± 0.015	2.053 ± 0.015	2.059 ± 0.015
	$\frac{\partial\gamma}{\partial z_l}$	-0.116 ± 0.053	-0.165 ± 0.064	-0.232 ± 0.053
Fixed a(z) bins	γ_0	2.046 ± 0.017	2.049 ± 0.014	2.059 ± 0.013
	$\frac{\partial\gamma}{\partial a(z)}$	-0.107 ± 0.06	-0.144 ± 0.054	-0.259 ± 0.036
Direct	γ_0	2.054 ± 0.025	2.056 ± 0.024	2.068 ± 0.021
	$\frac{\partial\gamma}{\partial z_l}$	-0.173 ± 0.092	-0.176 ± 0.092	-0.274 ± 0.057

- The variation between reconstruction methods falls within the 1 σ region across different samples.
- In the following constraints, we will only use the distance reconstruction from ANN+SNIa

Direct method & summary

Single slope

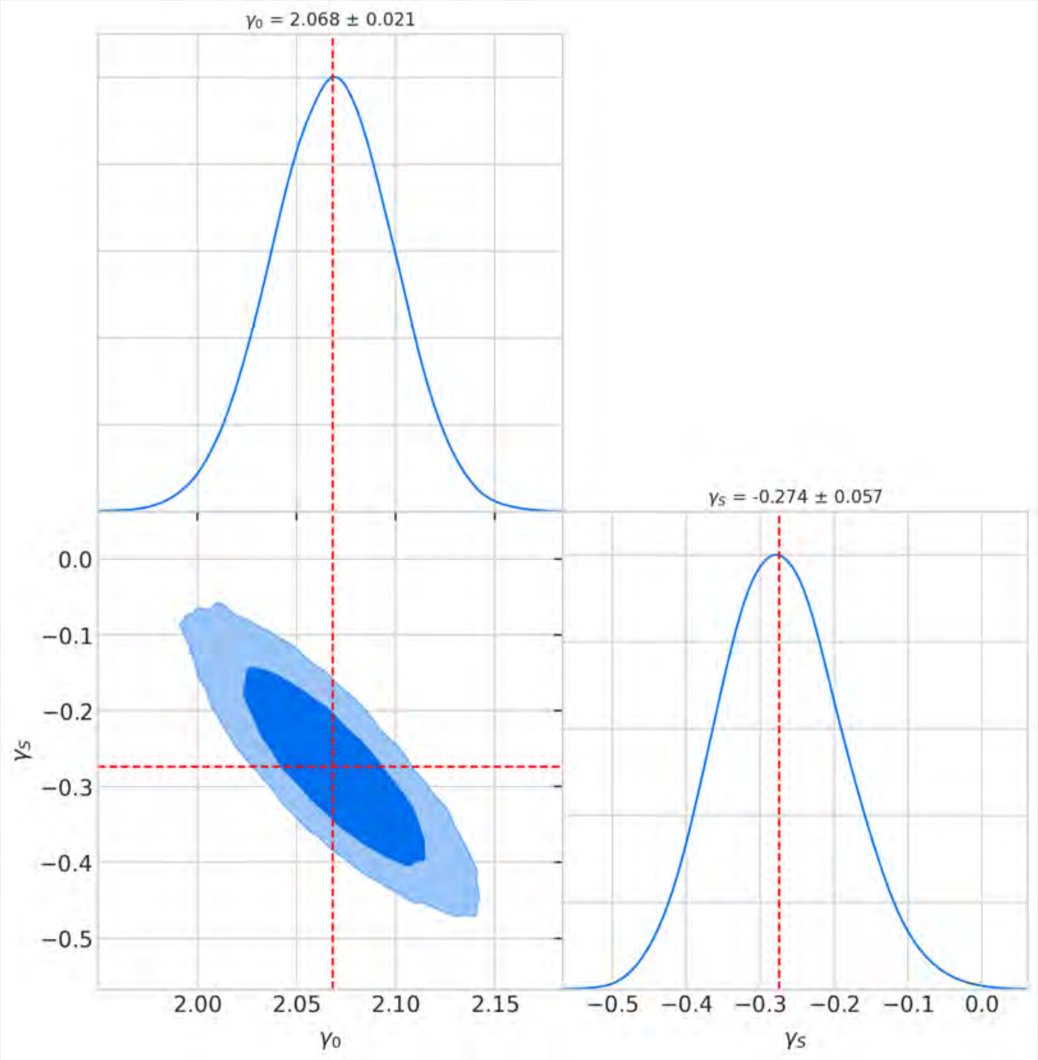

Approach	Parameters	GP34	ANN34	ANNlong
Individual	γ_0	2.048 ± 0.011	2.057 ± 0.011	2.068 ± 0.01
	$\frac{\partial\gamma}{\partial z_l}$	-0.131 ± 0.041	-0.142 ± 0.041	-0.226 ± 0.027
Fixed z bins	γ_0	2.044 ± 0.015	2.053 ± 0.015	2.059 ± 0.015
	$\frac{\partial\gamma}{\partial z_l}$	-0.116 ± 0.053	-0.165 ± 0.064	-0.232 ± 0.053
Fixed a(z) bins	γ_0	2.046 ± 0.017	2.049 ± 0.014	2.059 ± 0.013
	$\frac{\partial\gamma}{\partial a(z)}$	-0.107 ± 0.06	-0.144 ± 0.054	-0.259 ± 0.036
Direct	γ_0	2.054 ± 0.025	2.056 ± 0.024	2.068 ± 0.021
	$\frac{\partial\gamma}{\partial z_l}$	-0.173 ± 0.092	-0.176 ± 0.092	-0.274 ± 0.057

- The variation between reconstruction methods falls within the 1 σ region across different samples.
- In the following constraints, we will only use the distance reconstruction from ANN+SNIa

General SPL parameters

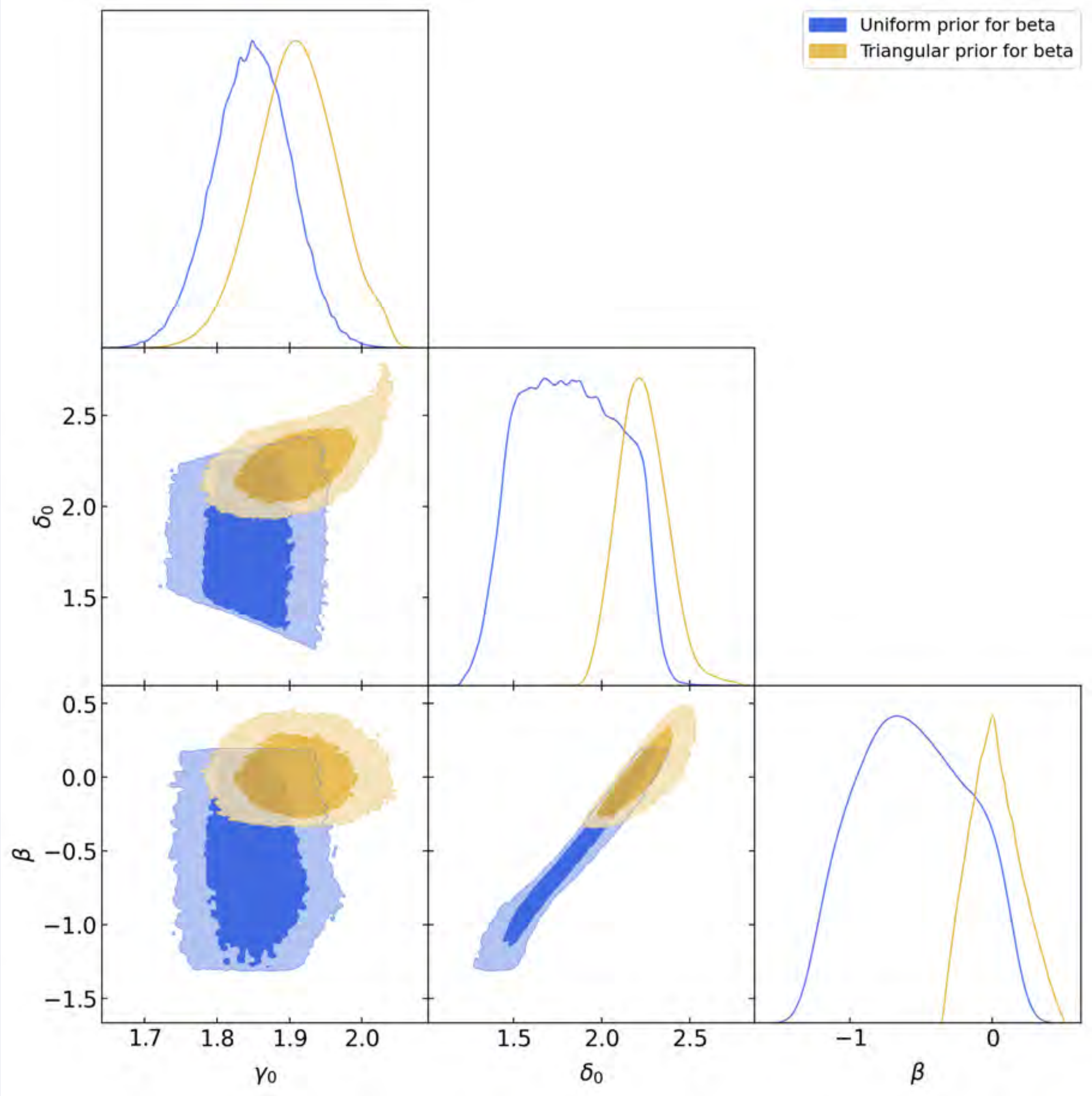

Breaking the degeneracy between density slope of luminous matter and the dynamical anisotropy.

General SPL parameters

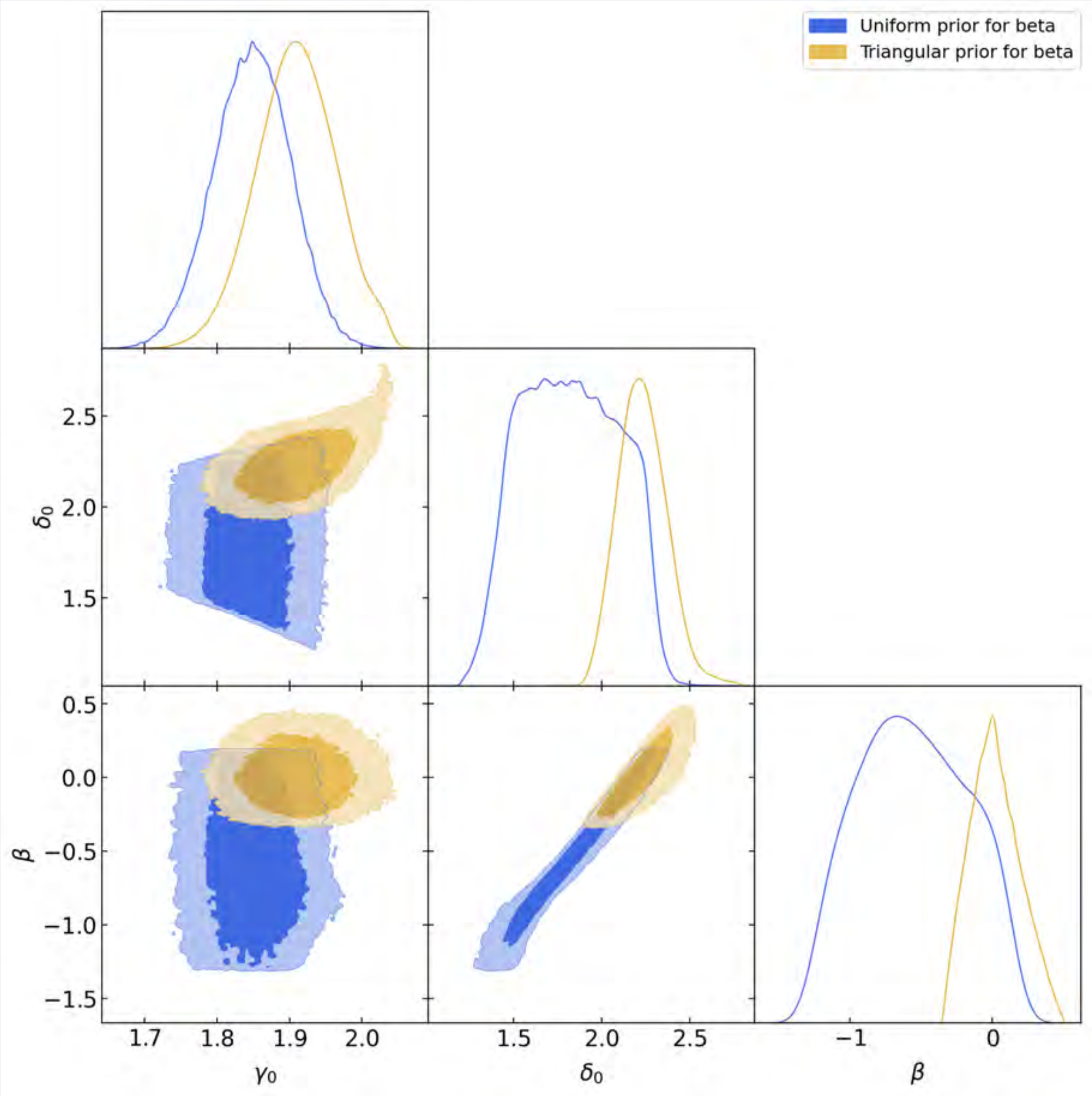

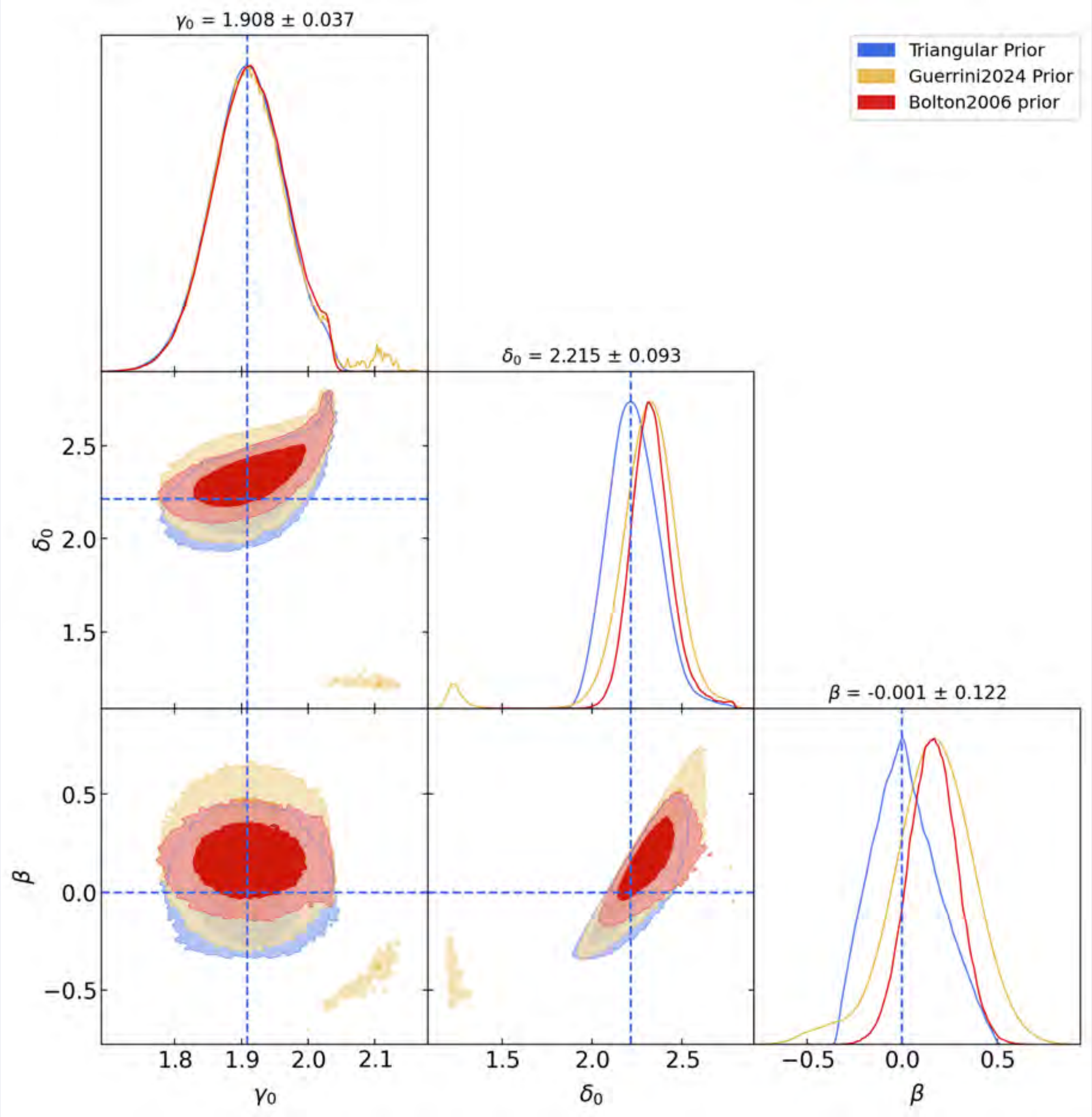

General evolving SPL parameters

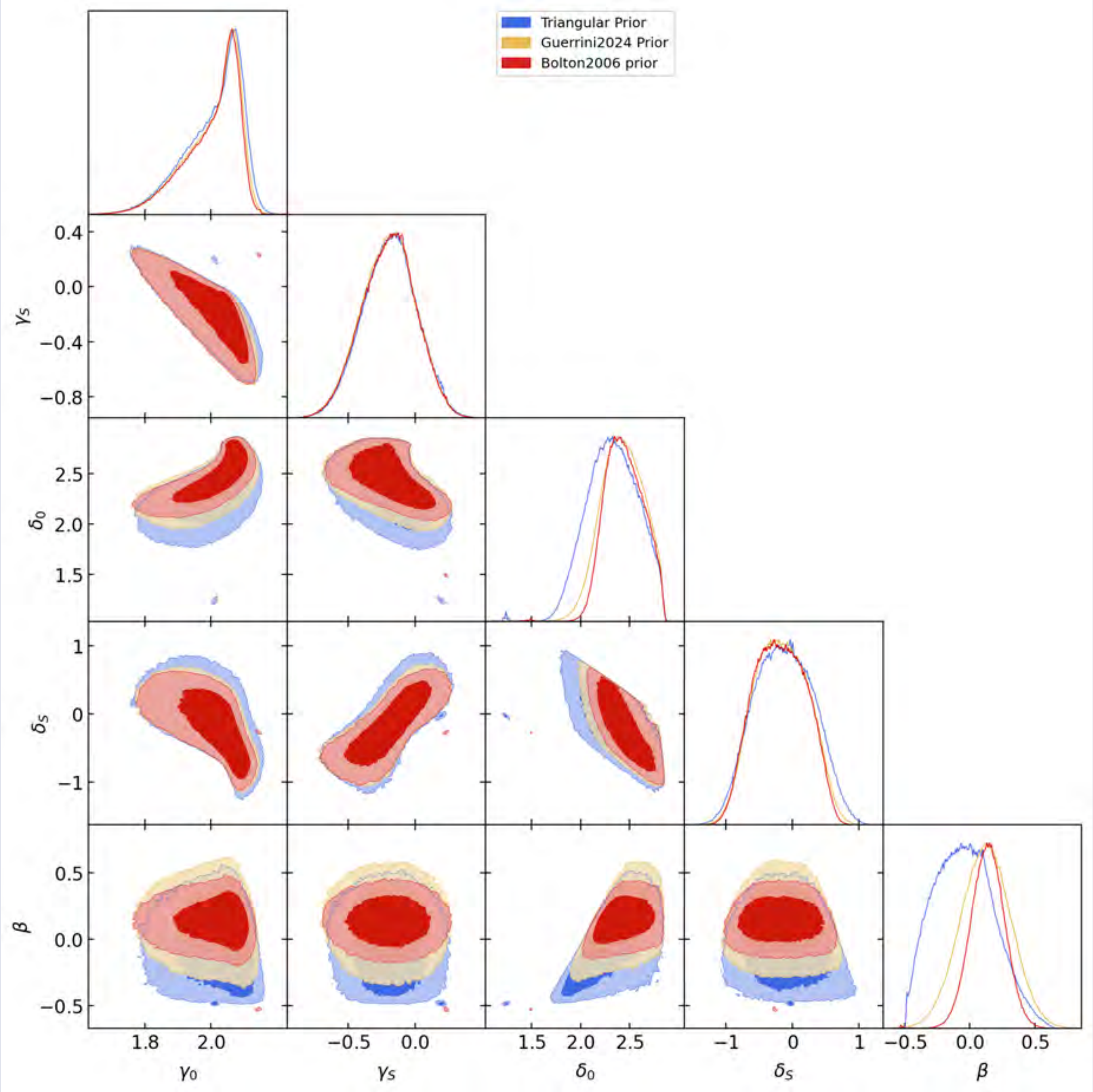

- The median value and the median absolute deviation recover the isothermal profile.
- The triangular prior works better.

Evolution model	β prior	parameters	AIC	BIC
Linear z evolution	Triangular prior Tri(-0.5,0.656,mode=0.102)	$\gamma_0 = 2.029 \pm 0.055$ $\gamma_s = -0.185 \pm 0.136$ $\delta_0 = 2.326 \pm 0.184$ $\delta_s = -0.128 \pm 0.324$ $\beta = -0.047 \pm 0.165$	121.0	136.1
	Gaussian prior $N(\mu = 0.22, \sigma^2 = 0.2^2)$	$\gamma_0 = 2.027 \pm 0.052$ $\gamma_s = -0.193 \pm 0.137$ $\delta_0 = 2.424 \pm 0.153$ $\delta_s = -0.174 \pm 0.294$ $\beta = 0.122 \pm 0.130$	131.7	146.7
	Gaussian prior $N(\mu = 0.18, \sigma^2 = 0.13^2)$	$\gamma_0 = 2.025 \pm 0.050$ $\gamma_s = -0.189 \pm 0.136$ $\delta_0 = 2.436 \pm 0.139$ $\delta_s = -0.187 \pm 0.291$ $\beta = 0.138 \pm 0.087$	133.7	148.7

General evolving SPL parameters

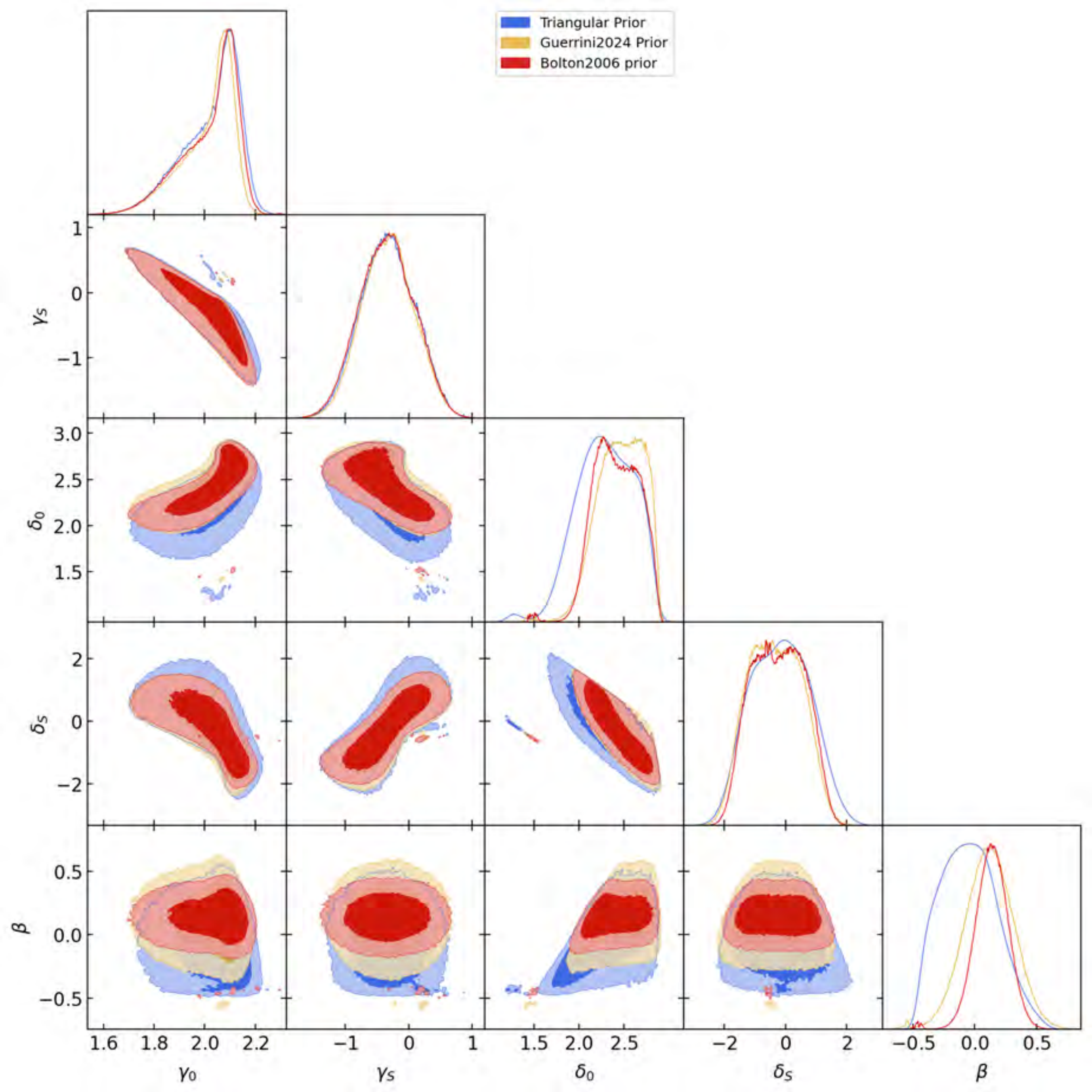

- The uncertainty of the luminous matter density slope constraint is larger than the linear evolution model.
- Gaussian prior performs better.

Linear a(z) evolution	Triangular prior Tri(-0.5,0.656,mode=0.102)	$\gamma_0 = 2.054 \pm 0.071$ $\gamma_s = -0.333 \pm 0.294$ $\delta_0 = 2.299 \pm 0.234$ $\delta_s = -0.156 \pm 0.722$ $\beta = -0.053 \pm 0.166$	115.6	130.7
	Gaussian prior $N(\mu = 0.22, \sigma^2 = 0.2^2)$	$\gamma_0 = 2.042 \pm 0.060$ $\gamma_s = -0.326 \pm 0.280$ $\delta_0 = 2.476 \pm 0.188$ $\delta_s = -0.348 \pm 0.658$ $\beta = 0.117 \pm 0.131$	113.3	128.3
	Gaussian prior $N(\mu = 0.18, \sigma^2 = 0.13^2)$	$\gamma_0 = 2.052 \pm 0.067$ $\gamma_s = -0.343 \pm 0.298$ $\delta_0 = 2.410 \pm 0.187$ $\delta_s = -0.234 \pm 0.664$ $\beta = 0.138 \pm 0.087$	181.9	197.0

Conclusions

- Under the simple power-law model, the density slope of lensing galaxies shows a negative evolution with increasing redshift, indicating that the mass distribution becomes more concentrated over time.
- With an appropriate prior for the dynamical anisotropy of the lensing galaxies, we recover a flatter density slope for total mass compared to luminous mass, aligning well with detailed modeling results. However, neglecting the evolution of the density slope leads to deviations from the isothermal profile for total mass.
- When considering various evolution models, the median value of the gamma posterior distribution supports the isothermal configuration. The findings indicate a slight negative evolution with increasing redshift for the total mass density slope, consistent with constraints from individual lensing systems under the simple power-law model. Nonetheless, the non-evolving scenario remains plausible within 1 sigma uncertainty.

THANKS FOR YOUR ATTENTION